Available online at www.sciencedirect.com
ScienceDirect
Computers & Fluids 37 (2008) 1209–1224
computers & fluids
www.elsevier.com/locate/compfluid

Behavior of upwind scheme in the low Mach number limit: III. Preconditioned dissipation for a five equation two phase model

Angelo Murrone [a,b,*], Hervé Guillard [b]

[a] CEA Cadarache, 13108 Saint-Paul-Lez-Durance, France
[b] INRIA, BP. 93, 06902 Sophia Antipolis Cedex, France

Received 5 April 2005; received in revised form 20 March 2006; accepted 1 December 2006
Available online 26 January 2008

Abstract

For single phase fluid models, like the Euler equations of compressible gas dynamics, upwind finite volume schemes suffer from a loss of accuracy when computing flows in the near incompressible regime. Preconditioning of the numerical dissipation is necessary to recover results consistent with the asymptotic behaviour of the continuous model. In this paper, we examine this situation for a two-phase flow model. We show that as in the single phase case, the numerical approximation has to be done carefully in the near incompressible regime. We propose to adapt the preconditioning strategy used for single phase problems and present numerical results that show the efficiency of this approach.

1. Introduction

Although two phase and multifluid flows are encountered in a large number of situations from hypersonic to almost zero velocity flows, in many cases, the computation of these flows is a low Mach problem. This is true for instance in the nuclear or petroleum industry in nominal conditions when one of the two phases is a liquid with very small compressibility coefficient forcing the flow velocity to be small. The modeling of these flows is an extremely difficult task and nowadays, there is no universal model to take into account all the experimental conditions. Instead a large collection of different type of models co-exist. In this paper, we are interested in modelings of the type described for instance in [12,9] in which the convective part of the model is described by an hyperbolic system. This includes a large variety of different models ranging from simple homogeneous [2] or drift flux models to sophisticated two pressure, two velocity models [9,1,10]. With a few exceptions, from a theoretical point of view, the behaviour for vanishing Mach number of these two-phase flows models is unknown. A consequence of this absence of understanding of the behaviour of these models when the Mach number goes to zero is that the numerical approximation methods used to solve them is generally based on standard finite volume or finite difference methods. The efficiency of these methods is well assessed for the numerical approximation of hyperbolic systems in transonic and supersonic regimes. However, for very subsonic flows, when these discretization methods are applied to standard one phase models as the Euler or Navier–Stokes equations, it is now well known that they suffer from efficiency and accuracy problems. Actually, it has even been proved in the case of the Euler equations that the numerical approximations produced by standard finite volume (FV) schemes of upwind type do not converge to the correct incompressible limit [5,4]. There is no reason to believe that the situation is different for hyperbolic two-phase flow models and that in the low Mach number regime, standard discretization can be used safely to compute these flows.

Indeed, for one of the simplest two-phase flows model, namely the homogeneous equilibrium model, it has been

* Corresponding author. Present address: ONERA, DEFA, 29 Avenue de la Division Leclerc, BP. 72, 92322 Châtillon, France. Tel.: +33 146734320.
E-mail addresses: angelo.murrone@onera.fr (A. Murrone), herve.guillard@inria.fr (H. Guillard).

0045-7930/$ - see front matter © 2008 Elsevier Ltd. All rights reserved.
doi:10.1016/j.compfluid.2006.12.010

shown in [2,16] that FV upwind schemes exhibit the same type of accuracy problems than in the one phase context. In this paper, we investigate this situation for a more complex two-phase flow model, namely the five-equation model introduced in [6,8]. This model has been used for detonation studies in [6,17]. In [8], we have shown that it can also be used for some low Mach interface and two-phase flows problems. Our aim, here is to show that in the low Mach number regime, the numerical approximation of this model has to be done carefully if one wants to avoid a loss of accuracy. Fortunately, we will also show that due to the mathematical structure of this model, the same recipe than in the case of the one-phase Euler equations can be applied and that preconditioning the numerical dissipation allows to recover a correct asymptotic behaviour when the Mach number goes to zero.

For the more complex non-equilibrium two-pressure and two velocity models of the type described for instance in [9,1,10], the situation is far from being understood. Actually, in contrast with the single velocity and pressure model considered in this paper, these models are governed by several (at least 4) non-dimensional numbers and therefore can experience a large number of different asymptotic regimes. The present work is therefore a step in the comprehension of the low Mach number behaviour of two-phase models but a lot of complex questions remain unanswered.

The summary of this work is as follows. In Section 2, we perform an asymptotic analysis of the model in the low Mach number limit. The purpose of this section is to identify the correct limit equation that the solutions satisfy when the Mach number goes to zero. Using a single time asymptotic analysis, we show that for this incompressible limit, as for the one-phase Euler equations, pressure fluctuations scale with the square of the Mach number. Then in Section 3, we propose an implicit numerical scheme based on a Godunov type solver. This numerical scheme uses the solution of a preconditioned Riemann solver to enable a correct asymptotic behaviour of the numerical solution. Following the recipe proposed for the Euler equations in [5,4], this preconditioned Riemann solver is built using the close similarity between the mathematical structure of this model and the one of the one-phase Euler equations. Finally in Section 4, we present a set of numerical experiments which show that this preconditioning strategy allows to recover accurate results when computing low Mach number flows with this model.

2. The continuous problem

The purpose of this section is to identify the limit equations and the asymptotic behaviour of the solutions of a two phase one-velocity, one-pressure model in the limit of vanishing low Mach number. Although this model describes the two phase medium by a single velocity and a single pressure, it retains two phase densities *and* a volume fraction for the description of the thermodynamical state of the fluid. Consequently, this model possesses two entropies (and two temperatures). This allows a richer description of the fluid than with the classical multicomponent Euler equations (that possesses a single temperature) and can have some advantages when the thermodynamics of the two fluids are very different. In term of conservative variables ${}^t(\alpha_1\rho_1, \alpha_2\rho_2, \rho\boldsymbol{u}, \rho e, \alpha_1)$, this system can be written as

$$\frac{\partial \alpha_1\rho_1}{\partial t} + \operatorname{div}(\alpha_1\rho_1\boldsymbol{u}) = 0 \tag{1.1}$$

$$\frac{\partial \alpha_2\rho_2}{\partial t} + \operatorname{div}(\alpha_2\rho_2\boldsymbol{u}) = 0 \tag{1.2}$$

$$\frac{\partial \rho\boldsymbol{u}}{\partial t} + \operatorname{div}(\rho\boldsymbol{u}\otimes\boldsymbol{u}) + \nabla p = 0 \tag{1.3}$$

$$\frac{\partial \rho e}{\partial t} + \operatorname{div}(\rho e + p)\boldsymbol{u} = 0 \tag{1.4}$$

$$\frac{\partial \alpha_1}{\partial t} + \boldsymbol{u}\cdot\nabla\alpha_1 = \alpha_1\alpha_2\frac{\rho_2 a_2^2 - \rho_1 a_1^2}{\sum_{k=1}^{2}\alpha_{k'}\rho_k a_k^2}\operatorname{div}\boldsymbol{u} \tag{1.5}$$

Notations are classical. $k = (1,2)$ stand for the two phases and $k' = (2,1)$ for $k = (1,2)$. Then α_k are the volume fractions $(\alpha_1 + \alpha_2 = 1)$, ρ_k the phase densities, $\boldsymbol{u}$ the vector velocity, and p the pressure. Then $\rho = \sum_{k=1}^{2}\alpha_k\rho_k$ stands for the mixture density and e the specific total energy is defined by $e = \varepsilon + \boldsymbol{u}^2/2$ while the specific internal energy ε is given by the relation $\rho\varepsilon = \sum_{k=1}^{2}\alpha_k\rho_k\varepsilon_k(p,\rho_k)$.

This model has been proposed for instance in [12,17,8] and can be obtained from an asymptotic analysis in the limit of zero relaxation time of the Baer–Nunziato two velocity, two-pressure model (see for instance [8]). Its mathematical properties are studied in [8] where it is shown that its structure is very close to the one of the one-phase Euler equations. Our aim, now is to perform an asymptotic analysis of this system when the Mach number tends to zero. Before that, let us recall the situation for the one-phase Euler equations: if the initial pressure field scales with the square of the Mach number: $p(\boldsymbol{x},0) = p^0 + Ma_*^2 p^2(\boldsymbol{x})$, and if the velocity at time $t = 0$ is close to a divergence free field in the sense that $\boldsymbol{u}(\boldsymbol{x},0) = \boldsymbol{u}^0(\mathbf{x}) + Ma_*\boldsymbol{u}^1(\boldsymbol{x})$ with $\operatorname{div}\boldsymbol{u}^0 = 0$, then it is known that solutions of the Euler equations for compressible flows remain uniformly bounded as the Mach number tends to zero, and the limit solutions satisfy the equations for incompressible flows:

$$\rho\left(\frac{\partial \boldsymbol{u}}{\partial t} + \operatorname{div}(\mathbf{u}\otimes\boldsymbol{u})\right) + \nabla\pi = 0 \tag{2.1}$$

$$\operatorname{div}(\boldsymbol{u}) = 0 \tag{2.2}$$

In the sequel, we will establish the same type of results for the model (1). For the sake of simplicity, we first rewrite system (1) using the pressure as independent variable instead of the total energy. The equation governing the evolution of the pressure is

$$\frac{\partial p}{\partial t} + \boldsymbol{u}\cdot\nabla p + \rho\hat{a}^2\operatorname{div}\boldsymbol{u} = 0 \tag{3}$$

In this last equation, we have introduced the averaged sound speed $\hat{a}$ defined by (see for instance [12,17,8])

$$\frac{1}{\rho\hat{a}^2} = \sum_{k=1}^{2} \frac{\alpha_k}{\rho_k a_k^2} \tag{4}$$

Formula (4) is the celebrated Wallis (or Woods) equilibrium sound speed well known in the two-phase flow literature (see e.g [12]).

The first step of the analysis is to perform a change of variables using non-dimensional variables instead of dimensional ones. Let $\rho_{\text{ref}} = \max[\rho(\boldsymbol{x},0)], u_{\text{ref}}^2 = \max[\boldsymbol{u}^2(\boldsymbol{x},0)]$ and let the sound speed scale $\hat{a}_{\text{ref}}$ be defined by: $\hat{a}_{\text{ref}} = \max[\hat{a}(\boldsymbol{x},0)]$.

Introducing the non-dimensionalized variables:

$$\tilde{\rho}_k = \frac{\rho_k}{\rho_{\text{ref}}} \quad \tilde{\boldsymbol{u}} = \frac{\boldsymbol{u}}{u_{\text{ref}}} \quad \tilde{p} = \frac{p}{\rho_{\text{ref}}\hat{a}_{\text{ref}}^2} \quad \tilde{\alpha}_k = \alpha_k \quad \tilde{\boldsymbol{x}} = \frac{\boldsymbol{x}}{\delta_{\text{ref}}} \quad \tilde{t} = \frac{t u_{\text{ref}}}{\delta_{\text{ref}}} \tag{5}$$

with δ_{ref} an arbitrary length scale, system (1) becomes:

$$\frac{\partial\tilde{\alpha}_1\tilde{\rho}_1}{\partial t} + \operatorname{div}(\tilde{\alpha}_1\tilde{\rho}_1\tilde{\boldsymbol{u}}) = 0 \tag{6.1}$$

$$\frac{\partial\tilde{\alpha}_2\tilde{\rho}_2}{\partial t} + \operatorname{div}(\tilde{\alpha}_2\tilde{\rho}_2\tilde{\boldsymbol{u}}) = 0 \tag{6.2}$$

$$\frac{\partial\tilde{\rho}\tilde{\boldsymbol{u}}}{\partial t} + \operatorname{div}(\tilde{\rho}\tilde{\boldsymbol{u}}\otimes\tilde{\boldsymbol{u}}) + \frac{1}{Ma_*^2}\nabla\tilde{p} = 0 \tag{6.3}$$

$$\frac{\partial\tilde{p}}{\partial t} + \tilde{\boldsymbol{u}}\cdot\nabla\tilde{p} + \tilde{\rho}\tilde{\hat{a}}^2\operatorname{div}\tilde{\boldsymbol{u}} = 0 \tag{6.4}$$

$$\frac{\partial\tilde{\alpha}_1}{\partial t} + \tilde{\boldsymbol{u}}\cdot\nabla\tilde{\alpha}_1 = \tilde{\alpha}_1\tilde{\alpha}_2\frac{\tilde{\rho}_2\tilde{a}_2^2 - \tilde{\rho}_1\tilde{a}_1^2}{\sum_{k=1}^{2}\tilde{\alpha}_{k'}\tilde{\rho}_k\tilde{a}_k^2}\operatorname{div}\tilde{\boldsymbol{u}} \tag{6.5}$$

where $Ma_* = u_{\text{ref}}/\hat{a}_{\text{ref}}$ is the reference Mach number.

And we now look for solution of system (6) in the form of asymptotic expansion in power of the Mach number Ma_*:

$$(\tilde{.}) = (\tilde{.})^0 + Ma_*(\tilde{.})^1 + Ma_*^2(\tilde{.})^2 + \cdots \tag{7}$$

Introducing these expressions into system (6) and collecting terms with equal power of Ma_*, we obtain at order $1/Ma_*^2$ and $1/Ma_*$ (in the sequel, we have dropped the subscripts $\tilde{.}$ for convenience)

$$\nabla p^0 = 0 \tag{8.1}$$

$$\nabla p^1 = 0 \tag{8.2}$$

These equations imply that the pressure is constant in space up to fluctuations of order Ma_*^2. Thus we may write

$$p(\boldsymbol{x},t) = p^0(t) + Ma_*^2 p^2(\boldsymbol{x},t) \tag{9}$$

and this situation is then identical to the one obtained for the one-phase Euler equation.

Then introducing these results in the order 1 system, we get

$$\frac{\partial\alpha_1^0\rho_1^0}{\partial t} + \operatorname{div}(\alpha_1^0\rho_1^0\boldsymbol{u}^0) = 0 \tag{10.1}$$

$$\frac{\partial\alpha_2^0\rho_2^0}{\partial t} + \operatorname{div}(\alpha_2^0\rho_2^0\boldsymbol{u}^0) = 0 \tag{10.2}$$

$$\frac{\partial\rho^0\boldsymbol{u}^0}{\partial t} + \operatorname{div}(\rho^0\boldsymbol{u}^0\otimes\boldsymbol{u}^0) + \nabla p^2 = 0 \tag{10.3}$$

$$\frac{\mathrm{d}p^0}{\mathrm{d}t} + \rho^0(\hat{a}^0)^2\operatorname{div}\boldsymbol{u}^0 = 0 \tag{10.4}$$

$$\frac{\partial\alpha_1^0}{\partial t} + \boldsymbol{u}^0\cdot\nabla\alpha_1^0 = \alpha_1^0\alpha_2^0\frac{\rho_2^0(a_2^0)^2 - \rho_1^0(a_1^0)^2}{\sum_{k=1}^{2}\alpha_{k'}^0\rho_k^0(a_k^0)^2}\operatorname{div}\boldsymbol{u}^0 \tag{10.5}$$

To simplify, these equations, we note that in the presence of open boundaries, the thermodynamic pressure p^0 will be imposed and be equal to the exterior pressure. For the sake of simplicity, we assume that the exterior pressure does not change with time, and thus, the pressure p^0 will be a constant in space and time:

$$\frac{\mathrm{d}p^{\text{Ext}}}{\mathrm{d}t} = \frac{\mathrm{d}p^0}{\mathrm{d}t} = 0 \tag{11}$$

and the pressure equation (10.4) degenerates into:

$$\operatorname{div}\boldsymbol{u}^0 = 0 \tag{12}$$

Again, this situation is totally identical to the one of the one-phase Euler equation. Now, introducing relation (12) into the mass conservation equations (10.1) and (10.2) and the volume fraction equation (10.5), we get

$$\frac{\partial\rho_k^0}{\partial t} + \boldsymbol{u}^0\cdot\nabla\rho_k^0 = 0 \quad \text{and} \quad \frac{\partial\alpha_1^0}{\partial t} + \boldsymbol{u}^0\cdot\nabla\alpha_1^0 = 0 \tag{13}$$

Assuming that all particle paths come from regions with the same phase densities, we conclude that $\rho_k^0 = \text{Cte}$ and thus the set of equations that governs the evolution of the variables ${}^t(\alpha_1\rho_1, \alpha_2\rho_2, \rho\boldsymbol{u}, \rho e, \alpha_1)$ is asymptotically in the limit $Ma_* \to 0$

$$\rho_1 = \text{Cte} \tag{14.1}$$

$$\rho_2 = \text{Cte} \tag{14.2}$$

$$\frac{\partial\boldsymbol{u}}{\partial t} + \operatorname{div}(\boldsymbol{u}\otimes\boldsymbol{u}) + \frac{1}{\rho(\alpha_1)}\nabla p = 0 \tag{14.3}$$

$$\operatorname{div}\boldsymbol{u} = 0 \tag{14.4}$$

$$\frac{\partial\alpha_1}{\partial t} + \boldsymbol{u}\cdot\nabla\alpha_1 = 0 \tag{14.5}$$

where the mixture density $\rho(\alpha_1) = \alpha_1\rho_1 + (1-\alpha_1)\rho_2$ depends only on the volume fraction α_1 which is simply advected at the velocity $\boldsymbol{u}$ of the flow. Note the close similarity with the one phase incompressible Euler equation (2).

3. Numerical approximation

System (1) is not a conservative system due to the evolution equation for the volume fraction

$$\frac{\partial \alpha_1}{\partial t} + \boldsymbol{u}\cdot\nabla\alpha_1 = \alpha_1\alpha_2 \frac{\rho_2 a_2^2 - \rho_1 a_1^2}{\sum_{k=1}^{2}\alpha_{k'}\rho_k a_k^2}\mathrm{div}\boldsymbol{u} \tag{15}$$

where $k' = (2,1)$ for $k = (1,2)$. In the numerical approximation used in this paper, we rewrite this equation as

$$\frac{\partial \alpha_1}{\partial t} + \mathrm{div}(\alpha_1\mathbf{u}) + B(\boldsymbol{Q})\mathrm{div}\boldsymbol{u} = 0 \quad \text{with} \quad B(\boldsymbol{Q}) = \frac{-\alpha_1\rho_2 a_2^2}{\sum_{k=1}^{2}\alpha_{k'}\rho_k a_k^2} \tag{16}$$

Then let $\boldsymbol{Q} = {}^t(\alpha_1\rho_1, \alpha_2\rho_2, \rho\boldsymbol{u}, \rho e, \alpha_1)$ be the set of "conservative"[1] variables. With this definition, the system (1) can be written as

$$\frac{\partial \boldsymbol{Q}}{\partial t} + \mathrm{div}\boldsymbol{F}(\boldsymbol{Q}) + \mathrm{div}\boldsymbol{u}\boldsymbol{B}(\boldsymbol{Q}) = 0 \tag{17}$$

where $\boldsymbol{B}(\boldsymbol{Q}) = {}^t(0,0,\mathbf{0},0,B(\boldsymbol{Q}))$. Integrating this equation on a cell C_i gives

$$A_i\frac{\partial \boldsymbol{Q}_i}{\partial t} + \int_{\partial C_i}\boldsymbol{F}(\boldsymbol{Q})\cdot\boldsymbol{n}\mathrm{d}l + \int_{C_i}\boldsymbol{B}(\boldsymbol{Q})\mathrm{div}\boldsymbol{u}\,\mathrm{d}\Omega = 0 \quad \text{for } i \in \{1,\ldots,N\} \tag{18}$$

where N is the number of cells and A_i is the volume of the cell C_i. Defining $v(i)$ as the set of cells C_j that share an edge with C_i and defining $\partial C_{ij} = \partial C_i \cap \partial C_j$, we approximate (18) by the following expression:

$$A_i\frac{\partial \boldsymbol{Q}_i}{\partial t} + \sum_{j\in v(i)}\int_{\partial C_{ij}}\boldsymbol{F}(\boldsymbol{Q})\cdot\boldsymbol{n}\,\mathrm{d}l + \langle\boldsymbol{B}\rangle_i\sum_{j\in v(i)}\int_{\partial C_{ij}}\boldsymbol{u}\cdot\boldsymbol{n}\,\mathrm{d}l = 0 \tag{19}$$

where $\langle\boldsymbol{B}\rangle_i$ is some average of $\boldsymbol{B}$ on the cell C_i. In this work, we have used $\langle\boldsymbol{B}\rangle_i = \boldsymbol{B}(\boldsymbol{Q}_i)$ or $\langle\boldsymbol{B}\rangle_i = \sum_{j\in v(i)}\boldsymbol{B}(\boldsymbol{Q}^*_{ij})/\sum_{j\in v(i)}1$ with no noticeable difference. Then the surface integrals appearing in (19) are computed by a one-point formula to yield

$$A_i\frac{\partial \boldsymbol{Q}_i}{\partial t} + \sum_{j\in v(i)}\|\boldsymbol{n}_{ij}\|(\langle\boldsymbol{F}(\boldsymbol{Q})\cdot\boldsymbol{n}\rangle_{ij} + \langle\boldsymbol{B}\rangle_i\langle\boldsymbol{u}\cdot\boldsymbol{n}\rangle_{ij}) = 0 \tag{20}$$

where $\boldsymbol{n}_{ij} = \int_{\partial C_{ij}}\boldsymbol{n}\,\mathrm{d}l$ is the integral of the normal vector of the interface and $\langle\boldsymbol{F}(\boldsymbol{Q})\cdot\boldsymbol{n}\rangle_{ij}$ (resp. $\langle\boldsymbol{u}\cdot\boldsymbol{n}\rangle_{ij}$) denotes some averages of $\boldsymbol{F}(\boldsymbol{Q})\cdot\boldsymbol{n}$ (resp. $\boldsymbol{u}\cdot\boldsymbol{n}$) on ∂C_{ij}. In this work, we use a Godunov type solver and define these average values by

$$\begin{aligned}\langle\boldsymbol{F}(\boldsymbol{Q})\cdot\boldsymbol{n}\rangle_{ij} &= \boldsymbol{F}(\boldsymbol{Q}^*_{ij})\cdot\boldsymbol{\eta}_{ij}\\ \langle\boldsymbol{u}\cdot\boldsymbol{n}\rangle_{ij} &= \boldsymbol{u}^*_{ij}\cdot\boldsymbol{\eta}_{ij}\end{aligned} \tag{21}$$

where $\boldsymbol{\eta}_{ij} = \boldsymbol{n}_{ij}/\|\boldsymbol{n}_{ij}\|$ and $\boldsymbol{Q}^*_{ij}$ is the exact or approximate solution of an approximate Riemann problem between the states $\boldsymbol{Q}_i$ and $\boldsymbol{Q}_j$ and $\boldsymbol{u}^*_{ij}\cdot\boldsymbol{\eta}_{ij}$ is the corresponding normal velocity. In low Mach number situations, the correct definition of this Riemann problem is crucial for the accuracy of the numerical approximation. In the following section, we describe how this Riemann problem is set.

[1] Although α_1 is not a conserved quantity, we will use this terminology for convenience.

3.1. Preconditioned Riemann problem

In standard upwind method, the Riemann problem defining the state $\boldsymbol{Q}^*_{ij}$ is based on the original differential system (1). Thus, let $\boldsymbol{q} = \boldsymbol{q}(\boldsymbol{Q})$ denote some change of variables such that $R = \partial\boldsymbol{q}/\partial\boldsymbol{Q}$ is invertible and define a local basis $(\boldsymbol{\eta}_{\mathrm{LR}}, \boldsymbol{\eta}^{\perp}_{\mathrm{LR}})$ of unit vectors, respectively, normal and tangential to the interface. In term of these new variables, the Riemann problem between the states $\boldsymbol{Q}_i = \boldsymbol{Q}_{\mathrm{L}}$ and $\boldsymbol{Q}_j = \boldsymbol{Q}_{\mathrm{R}}$ that will allow to compute $\boldsymbol{Q}^*_{ij} = \boldsymbol{Q}(x/t = 0; \boldsymbol{Q}_i, \boldsymbol{Q}_j)$ is defined by

$$\begin{aligned}&\frac{\partial\tilde{\boldsymbol{q}}}{\partial t} + A_{\mathrm{e}}(\tilde{\boldsymbol{q}})\frac{\partial\tilde{\boldsymbol{q}}}{\partial x} = 0\\ &\tilde{\boldsymbol{q}}(x,0) = \begin{cases}\tilde{\boldsymbol{q}}_{\mathrm{L}} & \text{if } x < 0\\ \tilde{\boldsymbol{q}}_{\mathrm{R}} & \text{if } x > 0\end{cases}\end{aligned} \tag{22}$$

where $\tilde{\boldsymbol{q}} = \theta\boldsymbol{q}$ is the projection of the vector $\boldsymbol{q}$ in the local basis $(\boldsymbol{\eta}_{\mathrm{LR}}, \boldsymbol{\eta}^{\perp}_{\mathrm{LR}})$ and where $A_{\mathrm{e}} = R[\partial(\boldsymbol{F}(\boldsymbol{Q})\cdot\boldsymbol{\eta}_{\mathrm{LR}})/\partial\boldsymbol{Q} + \boldsymbol{B}(\boldsymbol{Q})\partial(\boldsymbol{u}\cdot\boldsymbol{\eta}_{\mathrm{LR}})/\partial\boldsymbol{Q}]R^{-1}$. However, in the low Mach number limit, for the one-phase Euler equations, this strategy leads to numerical schemes that do not have the correct asymptotic behaviour. This situation is explained in detail in [4] where it is shown that the trouble comes from the fact that the interface pressure computed by the Riemann solver based on (22) contains pressure fluctuations of order Mach even if the initial data contain fluctuations that scale with the square of the Mach number. In [4], to overcome this difficulty, we proposed to solve instead of the Riemann problem (22) based on the original differential system, to solve a *preconditioned* Riemann problem. We propose here to apply the same strategy to the system (1). The transposition of this strategy to system (1) is greatly simplified by the fact that the mathematical structure of this model is very close to the one of the Euler equations. Actually, it is shown in [8] that in term of "entropic" variables $\boldsymbol{q} = {}^t(p, \boldsymbol{u}, s_1, s_2, Y_1)$ system (1) can be written as

$$\frac{\mathrm{D}p}{\mathrm{D}t} + \rho\hat{a}^2\mathrm{div}\boldsymbol{u} = 0 \tag{23.1}$$

$$\frac{\mathrm{D}\boldsymbol{u}}{\mathrm{D}t} + \frac{1}{\rho}\nabla p = 0 \tag{23.2}$$

$$\frac{\mathrm{D}s_1}{\mathrm{D}t} = 0 \tag{23.3}$$

$$\frac{\mathrm{D}s_2}{\mathrm{D}t} = 0 \tag{23.4}$$

$$\frac{\mathrm{D}Y_1}{\mathrm{D}t} = 0 \tag{23.5}$$

where we have introduced s_k for the phase entropies, $Y_k = \alpha_k\rho_k/\rho$ for the mass fraction and the notation $D/Dt = \partial/\partial t + \boldsymbol{u}\cdot\nabla$ for the material derivative. The expressions of the matrices R et R^{-1} when $\boldsymbol{q}$ is the entropic vector variables are given in Appendix B.

Using this form of the equations, it becomes obvious that the only change with the one-phase Euler equations is that we have now three linearly degenerate fields instead of a single one. However, the formal structure of the two

systems are identical. Therefore, extending the method used in [4], we define a "Turkel" preconditioner [14] by

$$P_e(\beta) = \mathrm{diag}(\beta^2, Id_n, 1, 1, 1) \tag{24}$$

where Id_n is the n-dimensional identity matrix (n is the space dimension) and β a parameter of the order of the Mach number. For the one-phase Euler equations, we recall that the Turkel preconditioner in entropic variables is defined by $P_e(\beta) = \mathrm{diag}(\beta^2, Id_n, 1)$. With this definition, as in [4], instead of solving (22), we will solve a *preconditioned* Riemann problem defined as

$$\begin{aligned} &\frac{\partial \tilde{\boldsymbol{q}}}{\partial t} + P_e(\beta) A_e(\tilde{\boldsymbol{q}}) \frac{\partial \tilde{\boldsymbol{q}}}{\partial x} = 0 \\ &\tilde{\boldsymbol{q}}(x,0) = \begin{cases} \tilde{\boldsymbol{q}}_L & \text{if } x < 0 \\ \tilde{\boldsymbol{q}}_R & \text{if } x > 0 \end{cases} \end{aligned} \tag{25}$$

Note that using $\beta = 1$ i.e $P_e(\beta) = Id$ will simply result in a non-preconditioned scheme, this allows to recover a standard approximation for transonic flows.

The matrix $P_e(\beta)A_e(\tilde{\boldsymbol{q}})$ is given by

$$P_e(\beta)A_e(\tilde{\boldsymbol{q}}) = \begin{pmatrix} \beta^2 v_n & \beta^2 \rho \hat{a}^2 & 0 & 0 & 0 & 0 \\ 1/\rho & v_n & 0 & 0 & 0 & 0 \\ 0 & 0 & v_n Id_{n-1} & 0 & 0 & 0 \\ 0 & 0 & 0 & v_n & 0 & 0 \\ 0 & 0 & 0 & 0 & v_n & 0 \\ 0 & 0 & 0 & 0 & 0 & v_n \end{pmatrix} \tag{26}$$

where $v_n = \boldsymbol{u} \cdot \boldsymbol{\eta}_{LR}$. This matrix is diagonalizable. In 2-D, for instance, forming the characteristic equation $(v_n - \lambda)^4 (\lambda^2 - (1+\beta^2)v_n\lambda + \beta^2(v_n^2 - \hat{a}^2)) = 0$, we get three distinct real eigenvalues:

$$\begin{cases} \lambda_1(\tilde{\boldsymbol{q}}) = \frac{1}{2}\left[(1+\beta^2)v_n - \sqrt{X}\right] \\ \lambda_2(\tilde{\boldsymbol{q}}) = \lambda_3(\tilde{\boldsymbol{q}}) = \lambda_4(\tilde{\boldsymbol{q}}) = \lambda_5(\tilde{\boldsymbol{q}}) = v_n \\ \lambda_6(\tilde{\boldsymbol{q}}) = \frac{1}{2}\left[(1+\beta^2)v_n + \sqrt{X}\right] \end{cases} \tag{27}$$

where we have introduced the parameter $X = [(1-\beta^2)v_n]^2 + 4\beta^2\hat{a}^2$. The associated right eigenvectors $r_i(\tilde{\boldsymbol{q}})$ (for $i \in \{1,\ldots,6\}$), that verify the relation $P_e(\beta)A_e(\tilde{\boldsymbol{q}})r_i(\tilde{\boldsymbol{q}}) = \lambda_i(\tilde{\boldsymbol{q}})r_i(\tilde{\boldsymbol{q}})$ can be, respectively, chosen as

$$\begin{aligned} r_1(\tilde{\boldsymbol{q}}) &= \begin{pmatrix} 1 \\ \frac{-s}{\beta^2\rho\hat{a}^2} \\ 0 \\ 0 \\ 0 \\ 0 \end{pmatrix} \quad r_2(\tilde{\boldsymbol{q}}) = \begin{pmatrix} 0 \\ 0 \\ 1 \\ 0 \\ 0 \\ 0 \end{pmatrix} \quad r_3(\tilde{\boldsymbol{q}}) = \begin{pmatrix} 0 \\ 0 \\ 0 \\ 1 \\ 0 \\ 0 \end{pmatrix} \\ r_4(\tilde{\boldsymbol{q}}) &= \begin{pmatrix} 0 \\ 0 \\ 0 \\ 0 \\ 1 \\ 0 \end{pmatrix} r_5(\tilde{\boldsymbol{q}}) = \begin{pmatrix} 0 \\ 0 \\ 0 \\ 0 \\ 0 \\ 1 \end{pmatrix} \quad r_6(\tilde{\boldsymbol{q}}) = \begin{pmatrix} 1 \\ \frac{-r}{\beta^2\rho\hat{a}^2} \\ 0 \\ 0 \\ 0 \\ 0 \end{pmatrix} \end{aligned} \tag{28}$$

where $r = \lambda_1 - v_n$ and $s = \lambda_6 - v_n$. We denote also by $l_i(\tilde{\boldsymbol{q}})$ (for $i \in \{1,\ldots,6\}$) the left eigenvectors which obey the relation ${}^t P_e(\beta)A_e(\tilde{\boldsymbol{q}})l_i(\tilde{\boldsymbol{q}}) = \lambda_i(\tilde{\boldsymbol{q}})l_i(\tilde{\boldsymbol{q}})$. After normalization of left and right eigenvectors to have ${}^t l_i(\tilde{\boldsymbol{q}}).r_j(\tilde{\boldsymbol{q}}) = \delta_{ij}$, we get

$$\begin{aligned} l_1(\tilde{\boldsymbol{q}}) &= \frac{-1}{\sqrt{X}} \begin{pmatrix} r \\ \beta^2\rho\hat{a}^2 \\ 0 \\ 0 \\ 0 \\ 0 \end{pmatrix} \quad l_2(\tilde{\boldsymbol{q}}) = \begin{pmatrix} 0 \\ 0 \\ 1 \\ 0 \\ 0 \\ 0 \end{pmatrix} \quad l_3(\tilde{\boldsymbol{q}}) = \begin{pmatrix} 0 \\ 0 \\ 0 \\ 1 \\ 0 \\ 0 \end{pmatrix} \\ l_4(\tilde{\boldsymbol{q}}) &= \begin{pmatrix} 0 \\ 0 \\ 0 \\ 0 \\ 1 \\ 0 \end{pmatrix} \quad l_5(\tilde{\boldsymbol{q}}) = \begin{pmatrix} 0 \\ 0 \\ 0 \\ 0 \\ 0 \\ 1 \end{pmatrix} \quad l_6(\tilde{\boldsymbol{q}}) = \frac{1}{\sqrt{X}} \begin{pmatrix} s \\ \beta^2\rho\hat{a}^2 \\ 0 \\ 0 \\ 0 \\ 0 \end{pmatrix} \end{aligned} \tag{29}$$

In the sequel we describe a preconditioned acoustic solver to approximately solve (25). More specifically, the numerical approximation of the Riemann problem (25) uses an extension of the acoustic solver described for instance in [13] for the single phase Euler equations. The idea of this solver is to use the known structure of the solution of the Riemann problem and to write linearized characteristic equations from the two sides of the contact discontinuity. The computation of the intersection of these linearized relations allows to get the velocity and pressure at the interface. To be more specific the approximate solution of the Riemann problem (25) that we consider consists of four constant states $\tilde{\boldsymbol{q}}_L, \tilde{\boldsymbol{q}}_L^*, \tilde{\boldsymbol{q}}_R^*$ and $\tilde{\boldsymbol{q}}_R$ where the velocities and pressures of the two states $\tilde{\boldsymbol{q}}_L^*, \tilde{\boldsymbol{q}}_R^*$ are equal: $u_L^* = u_R^* = u^*$ and $p_L^* = p_R^* = p^*$. To obtain u^*, p^*, we first transform the system of partial differential equations into ordinary differential equations by multiplying them with the left eigenvectors:

$${}^t l_i(\tilde{\boldsymbol{q}}) \cdot \left(\frac{\partial \tilde{\boldsymbol{q}}}{\partial t} + P_e(\beta) A_e(\tilde{\boldsymbol{q}}) \frac{\partial \tilde{\boldsymbol{q}}}{\partial x} \right) = 0 \tag{30}$$

This last relation can be immediately rewritten as

$$ {}^{t}l_i(\tilde{\boldsymbol{q}}) \cdot \left(\frac{\partial \tilde{\boldsymbol{q}}}{\partial t} + \lambda_i(\tilde{\boldsymbol{q}}) \frac{\partial \tilde{\boldsymbol{q}}}{\partial x} \right) = 0 \tag{31} $$

Linearizing (31) with respect to $\tilde{\boldsymbol{q}}_{\mathrm{L}}$ and $\tilde{\boldsymbol{q}}_{\mathrm{R}}$ we get

$$ \begin{cases} {}^{t}l_6(\tilde{\boldsymbol{q}}_{\mathrm{L}}) \cdot (\tilde{\boldsymbol{q}}^*_{\mathrm{L}} - \tilde{\boldsymbol{q}}_{\mathrm{L}}) = 0 \\ {}^{t}l_1(\tilde{\boldsymbol{q}}_{\mathrm{R}}) \cdot (\tilde{\boldsymbol{q}}^*_{\mathrm{R}} - \tilde{\boldsymbol{q}}_{\mathrm{R}}) = 0 \end{cases} \tag{32} $$

Due to the structure of the Riemann problem, these two relations can be solved for the common values $u^*_{\mathrm{L}} = u^*_{\mathrm{R}} = u^*$ and $p^*_{\mathrm{L}} = p^*_{\mathrm{R}} = p^*$ of the velocity and pressure on the two sides of the contact discontinuity. This gives after some algebraic manipulations:

$$ \begin{cases} u^* = \dfrac{C_{\mathrm{L}} u_{\mathrm{L}} + C_{\mathrm{R}} u_{\mathrm{R}}}{C_{\mathrm{L}} + C_{\mathrm{R}}} - \dfrac{p_{\mathrm{R}} - p_{\mathrm{L}}}{C_{\mathrm{L}} + C_{\mathrm{R}}} \\ p^* = \dfrac{C_{\mathrm{R}} p_{\mathrm{L}} + C_{\mathrm{L}} p_{\mathrm{R}}}{C_{\mathrm{L}} + C_{\mathrm{R}}} - \dfrac{C_{\mathrm{L}} C_{\mathrm{R}} (u_{\mathrm{R}} - u_{\mathrm{L}})}{C_{\mathrm{L}} + C_{\mathrm{R}}} \end{cases} \tag{33} $$

where C_{L} and C_{R} are given by

$$ \begin{cases} C_{\mathrm{L}} = \frac{1}{2}\rho_{\mathrm{L}} \left[\sqrt{\left[(1-\beta^2_{\mathrm{L}})u_{\mathrm{L}}\right]^2 + 4\beta^2_{\mathrm{L}}\hat{a}^2_{\mathrm{L}}} + (1-\beta^2_{\mathrm{L}})u_{\mathrm{L}} \right] \\ C_{\mathrm{R}} = \frac{1}{2}\rho_{\mathrm{R}} \left[\sqrt{\left[(1-\beta^2_{\mathrm{R}})u_{\mathrm{R}}\right]^2 + 4\beta^2_{\mathrm{R}}\hat{a}^2_{\mathrm{R}}} - (1-\beta^2_{\mathrm{R}})u_{\mathrm{R}} \right] \end{cases} \tag{34} $$

Note that in the transonic limit $\beta \to 1$, these formulas reduce to the ones given in [8] for non-preconditioned schemes. Then defining $(s_1)^*_{\mathrm{L}} = (s_1)_{\mathrm{L}}, (s_2)^*_{\mathrm{L}} = (s_2)_{\mathrm{L}}, (Y_1)^*_{\mathrm{L}} = (Y_1)_{\mathrm{L}}$ and $(s_1)^*_{\mathrm{R}} = (s_1)_{\mathrm{R}}, (s_2)^*_{\mathrm{R}} = (s_2)_{\mathrm{R}}, (Y_1)^*_{\mathrm{R}} = (Y_1)_{\mathrm{R}}$, the solution of the Riemann problem is given by

$$ \tilde{\boldsymbol{q}}\left(\frac{x}{t}, \tilde{\boldsymbol{q}}_{\mathrm{L}}, \tilde{\boldsymbol{q}}_{\mathrm{R}}\right) = \begin{cases} \tilde{\boldsymbol{q}}_{\mathrm{L}} & \text{if } \frac{x}{t} < \lambda_1(\tilde{\boldsymbol{q}}_{\mathrm{L}}) \\ \tilde{\boldsymbol{q}}^*_{\mathrm{L}} & \text{if } \lambda_1(\tilde{\boldsymbol{q}}_{\mathrm{L}}) < \frac{x}{t} < u^* \\ \tilde{\boldsymbol{q}}^*_{\mathrm{R}} & \text{if } u^* < \frac{x}{t} < \lambda_6(\tilde{\boldsymbol{q}}_{\mathrm{R}}) \\ \tilde{\boldsymbol{q}}_{\mathrm{R}} & \text{if } \lambda_6(\tilde{\boldsymbol{q}}_{\mathrm{R}}) < \frac{x}{t} \end{cases} \tag{35} $$

And we define the solution $\boldsymbol{Q}^*_{\mathrm{LR}}$ for the Godunov type scheme (21) by $\boldsymbol{Q}^*_{\mathrm{LR}}(\tilde{\boldsymbol{q}}^*_{\mathrm{LR}})$ with $\tilde{\boldsymbol{q}}^*_{\mathrm{LR}} = \tilde{\boldsymbol{q}}(x/t = 0, \tilde{\boldsymbol{q}}_{\mathrm{L}}, \tilde{\boldsymbol{q}}_{\mathrm{R}})$.

3.2. Implicit linearized scheme

Let us define

$$ \boldsymbol{\psi}(\boldsymbol{Q}_i, \boldsymbol{Q}_j) = \boldsymbol{F}(\boldsymbol{Q}^*_{ij}) \cdot \boldsymbol{\eta}_{ij} + \boldsymbol{B}(\boldsymbol{Q}_i)\boldsymbol{u}^*_{ij} \cdot \boldsymbol{\eta}_{ij} \tag{36} $$

$$ \begin{pmatrix} \frac{C_{\mathrm{L}}\mathrm{sgn}[\lambda_1]}{C_{\mathrm{L}}+C_{\mathrm{R}}} + \frac{C_{\mathrm{R}}\mathrm{sgn}[\lambda_6]}{C_{\mathrm{L}}+C_{\mathrm{R}}} & \frac{-C_{\mathrm{L}}C_{\mathrm{R}}\mathrm{sgn}[\lambda_1]}{C_{\mathrm{L}}+C_{\mathrm{R}}} + \frac{C_{\mathrm{L}}C_{\mathrm{R}}\mathrm{sgn}[\lambda_6]}{C_{\mathrm{L}}+C_{\mathrm{R}}} & 0 & 0 & 0 & 0 \\ \frac{-\mathrm{sgn}[\lambda_1]}{C_{\mathrm{L}}+C_{\mathrm{R}}} + \frac{\mathrm{sgn}[\lambda_6]}{C_{\mathrm{L}}+C_{\mathrm{R}}} & \frac{C_{\mathrm{R}}\mathrm{sgn}[\lambda_1]}{C_{\mathrm{L}}+C_{\mathrm{R}}} + \frac{C_{\mathrm{L}}\mathrm{sgn}[\lambda_6]}{C_{\mathrm{L}}+C_{\mathrm{R}}} & 0 & 0 & 0 & 0 \\ 0 & 0 & \mathrm{sgn}[u^*] & 0 & 0 & 0 \\ 0 & 0 & 0 & \mathrm{sgn}[u^*] & 0 & 0 \\ 0 & 0 & 0 & 0 & \mathrm{sgn}[u^*] & 0 \\ 0 & 0 & 0 & 0 & 0 & \mathrm{sgn}[u^*] \end{pmatrix} \tag{41} $$

where $\boldsymbol{Q}^*_{ij}$ is the conservative variable corresponding to the state $\tilde{\boldsymbol{q}}^*_{ij} = \tilde{\boldsymbol{q}}(x/t = 0, \tilde{\boldsymbol{q}}_i, \tilde{\boldsymbol{q}}_j)$ defined by Eq. (35) in term of "entropic" variables. A fully implicit first-order scheme using this expression would be defined by

$$ A_i \frac{\boldsymbol{Q}^{n+1}_i - \boldsymbol{Q}^n_i}{\Delta t} + \sum_{j \in v(i)} \|\boldsymbol{n}_{ij}\| \boldsymbol{\psi}(\boldsymbol{Q}^{n+1}_i, \boldsymbol{Q}^{n+1}_j) = 0 \tag{37} $$

However, this expression defines a non-algebraic system for $\boldsymbol{Q}_i$. A linear scheme of the same order of accuracy can be obtained by linearizing this expression around the state $\boldsymbol{Q}^n$ thanks to a Taylor development of the first-order. This gives the linear first-order scheme

$$ \begin{aligned} A_i \frac{\boldsymbol{Q}^{n+1}_i - \boldsymbol{Q}^n_i}{\Delta t} + \sum_{j \in v(i)} \|\boldsymbol{n}_{ij}\| \Big[\boldsymbol{\psi}(\boldsymbol{Q}^n_i, \boldsymbol{Q}^n_j) + \frac{\partial \boldsymbol{\psi}(\boldsymbol{Q}^n_i, \boldsymbol{Q}^n_j)}{\partial \boldsymbol{Q}^n_i} (\boldsymbol{Q}^{n+1}_i - \boldsymbol{Q}^n_i) \\ + \frac{\partial \boldsymbol{\psi}(\boldsymbol{Q}^n_i, \boldsymbol{Q}^n_j)}{\partial \boldsymbol{Q}^n_j} (\boldsymbol{Q}^{n+1}_j - \boldsymbol{Q}^n_j) \Big] = 0 \end{aligned} \tag{38} $$

However, in this equation ψ is a non-differentiable function because in (35), $\tilde{\boldsymbol{q}}(x/t, \tilde{\boldsymbol{q}}_{\mathrm{L}}, \tilde{\boldsymbol{q}}_{\mathrm{R}})$ is a discontinuous function and thus the linearization (38) is only an approximate one. This approximate linearization is done in this work as follows. First, neglecting the derivative of the non-conservative term $\boldsymbol{B}(\boldsymbol{Q}_i)$, we obtain

$$ \begin{cases} \frac{\partial \boldsymbol{\psi}(\boldsymbol{Q}^n_i, \boldsymbol{Q}^n_j)}{\partial \boldsymbol{Q}^n_i} \simeq \left[\frac{\partial \boldsymbol{F}(\boldsymbol{Q}^*_{ij}) \cdot \boldsymbol{\eta}_{ij}}{\partial \boldsymbol{Q}^*_{ij}} + \boldsymbol{B}(\boldsymbol{Q}^n_i) \frac{\partial \boldsymbol{u}^*_{ij} \cdot \boldsymbol{\eta}_{ij}}{\partial \boldsymbol{Q}^*_{ij}} \right] \frac{\partial \boldsymbol{Q}^*_{ij}}{\partial \boldsymbol{Q}^n_i} \quad \text{(a)} \\ \frac{\partial \boldsymbol{\psi}(\boldsymbol{Q}^n_i, \boldsymbol{Q}^n_j)}{\partial \boldsymbol{Q}^n_j} \simeq \left[\frac{\partial \boldsymbol{F}(\boldsymbol{Q}^*_{ij}) \cdot \boldsymbol{\eta}_{ij}}{\partial \boldsymbol{Q}^*_{ij}} + \boldsymbol{B}(\boldsymbol{Q}^n_i) \frac{\partial \boldsymbol{u}^*_{ij} \cdot \boldsymbol{\eta}_{ij}}{\partial \boldsymbol{Q}^*_{ij}} \right] \frac{\partial \boldsymbol{Q}^*_{ij}}{\partial \boldsymbol{Q}^n_j} \quad \text{(b)} \end{cases} \tag{39} $$

The expression for the Jacobian matrix $\partial(\boldsymbol{F}(\boldsymbol{Q}) \cdot \boldsymbol{\eta}_{ij})/\partial \boldsymbol{Q} + \boldsymbol{B}(\boldsymbol{Q})\partial(\boldsymbol{u} \cdot \boldsymbol{\eta}_{ij})/\partial \boldsymbol{Q}$ is given in Appendix A and the only remaining difficulty is to define $\partial \boldsymbol{Q}^*_{ij}/\partial \boldsymbol{Q}_i$ and $\partial \boldsymbol{Q}^*_{ij}/\partial \boldsymbol{Q}_j$. To approximate these derivatives, we first rewrite (35) for $x/t = 0$ under the form:

$$ \tilde{\boldsymbol{q}}^*_{\mathrm{LR}} = \frac{1}{2}\left[\tilde{\boldsymbol{q}}_{\mathrm{L}} + \tilde{\boldsymbol{q}}_{\mathrm{R}} + N \Delta \tilde{\boldsymbol{q}}_{\mathrm{LR}}\right] \tag{40} $$

where $\Delta \tilde{\boldsymbol{q}}_{\mathrm{LR}} = \tilde{\boldsymbol{q}}_{\mathrm{L}} - \tilde{\boldsymbol{q}}_{\mathrm{R}}$ and where N is the 6×6 matrix (with discontinuous coefficient given by formula (35)) which can be written under the following form with λ_1 and λ_6 standing for $\lambda_1(\tilde{\boldsymbol{q}}_{\mathrm{L}})$ and $\lambda_6(\tilde{\boldsymbol{q}}_{\mathrm{R}})$:

Taking into account the change of variables between conservative variables and "entropic" ones, we obtain that

the expression of the conservative variable $\boldsymbol{Q}^*_{\mathrm{LR}} = \boldsymbol{Q}(\tilde{\boldsymbol{q}}^*_{\mathrm{LR}})$ corresponding to the "entropic" variable $\tilde{\boldsymbol{q}}^*_{\mathrm{LR}}$ (40) can be approximated by

$$\boldsymbol{Q}^*_{\mathrm{LR}} \simeq \frac{1}{2}\left[\boldsymbol{Q}_{\mathrm{L}} + \boldsymbol{Q}_{\mathrm{R}} + \theta^{-1}R^{-1}NR\theta\Delta\boldsymbol{Q}_{\mathrm{LR}}\right] \tag{42}$$

where $R = \partial\boldsymbol{q}/\partial\boldsymbol{Q}$ and $R^{-1} = \partial\boldsymbol{Q}/\partial\boldsymbol{q}$ are the change of variables matrices between conservative variables $\boldsymbol{Q}$ and "entropic" ones $\boldsymbol{q}$ given in Appendix B, while θ and θ^{-1} are the rotation matrices that transform $\boldsymbol{Q}$ in the global space basis into $\tilde{\boldsymbol{Q}} = \theta\boldsymbol{Q} = {}^t(\alpha_1\rho_1, \alpha_2\rho_2, \rho v_{\mathrm{n}}, \rho v_{\mathrm{t}}, \rho e, \alpha_1)$ in the local basis $(\boldsymbol{\eta}, \boldsymbol{\eta}^{\perp})$ with $v_{\mathrm{n}} = \boldsymbol{u}\cdot\boldsymbol{\eta}$ and $v_{\mathrm{t}} = \boldsymbol{u}\cdot\boldsymbol{\eta}^{\perp}$ the normal and tangential components of the vector velocity to the local cell interface. With this approximation and locally freezing the matrix N, the expressions of $\partial\boldsymbol{Q}^*_{ij}/\partial\boldsymbol{Q}_i$ and $\partial\boldsymbol{Q}^*_{ij}/\partial\boldsymbol{Q}_j$ are, respectively, defined by

$$\begin{cases} \dfrac{\partial\boldsymbol{Q}^*_{ij}}{\partial\boldsymbol{Q}^n_i} \simeq \dfrac{1}{2}\left[Id + \theta^{-1}R^{-1}NR\theta\right] & \text{(a)} \\ \dfrac{\partial\boldsymbol{Q}^*_{ij}}{\partial\boldsymbol{Q}^n_j} \simeq \dfrac{1}{2}\left[Id - \theta^{-1}R^{-1}NR\theta\right] & \text{(b)} \end{cases} \tag{43}$$

where Id stands for the identity matrix. Finally, the first-order implicit backward scheme can be written as

$$\begin{aligned} A_i\frac{\boldsymbol{Q}^{n+1}_i - \boldsymbol{Q}^n_i}{\Delta t} &+ \sum_{j\in v(i)}\|\boldsymbol{n}_{ij}\|\left[\frac{1}{2}\left[\frac{\partial\boldsymbol{F}(\boldsymbol{Q}^*_{ij})\cdot\boldsymbol{\eta}_{ij}}{\partial\boldsymbol{Q}^*_{ij}} + \boldsymbol{B}(\boldsymbol{Q}^n_i)\frac{\partial\boldsymbol{u}^*_{ij}.\boldsymbol{\eta}_{ij}}{\partial\boldsymbol{Q}^*_{ij}}\right]\right. \\ &\times\left[Id + \theta^{-1}R^{-1}NR\theta\right](\boldsymbol{Q}^{n+1}_i - \boldsymbol{Q}^n_i) \\ &+\frac{1}{2}\left[\frac{\partial\boldsymbol{F}(\boldsymbol{Q}^*_{ij})\cdot\boldsymbol{\eta}_{ij}}{\partial\boldsymbol{Q}^*_{ij}} + \boldsymbol{B}(\boldsymbol{Q}^n_i)\frac{\partial\boldsymbol{u}^*_{ij}\cdot\boldsymbol{\eta}_{ij}}{\partial\boldsymbol{Q}^*_{ij}}\right] \\ &\times\left.\left[Id - \theta^{-1}R^{-1}NR\theta\right](\boldsymbol{Q}^{n+1}_j - \boldsymbol{Q}^n_j)\right] \\ &= -\sum_{j\in v(i)}\|\boldsymbol{n}_{ij}\|[\boldsymbol{F}(\boldsymbol{Q}^*_{ij})\cdot\boldsymbol{\eta}_{ij} + \boldsymbol{B}(\boldsymbol{Q}_i)\boldsymbol{u}^*_{ij}\cdot\boldsymbol{\eta}_{ij}] \end{aligned} \tag{44}$$

3.3. Extension to second-order space accuracy

Scheme (44) can be written under the form:

$$(M\Delta\boldsymbol{Q})_i = -\sum_{j\in v(i)}\|\boldsymbol{n}_{ij}\|\psi(\boldsymbol{Q}^n_i, \boldsymbol{Q}^n_j) \tag{45}$$

with $\Delta\boldsymbol{Q} = \boldsymbol{Q}^{n+1} - \boldsymbol{Q}^n$ and M is the matrix defined by Eq. (44). This scheme is only first-order accurate in time and space. To increase the order of accuracy of the scheme, we can change in the definition of the Riemann problem (25), the interface values $\boldsymbol{Q}_{\mathrm{L}} = \boldsymbol{Q}_i$ and $\boldsymbol{Q}_{\mathrm{R}} = \boldsymbol{Q}_j$ by linearly reconstructed states according to a MUSCL (Monotonic Upwind Scheme for Conservation Laws) [15] procedure. However, this reconstruction will increase the bandwidth of the matrix M and the linear system (45) will become more difficult to store and to solve. Therefore, although, formally the resulting scheme will be still first-order accurate, we will use instead of (45), the time-advancing scheme:

$$(M\Delta\boldsymbol{Q})_i = -\sum_{j\in v(i)}\|\boldsymbol{n}_{ij}\|\psi(\boldsymbol{Q}^n_{ij}, \boldsymbol{Q}^n_{ji}) \tag{46}$$

where $\boldsymbol{Q}_{ij}$ and $\boldsymbol{Q}_{ji}$ are reconstructed values on the two side of the interface between cells i and j while M is still first-order accurate and defined by Eq. (45). Numerical experiments show that although still formally first-order accurate, this procedure gives much more accurate results than the basic first-order scheme (45). The MUSCL procedure used here is the one derived for unstructured triangulation meshes in [3]. Here, instead of using the conservative variables $\boldsymbol{Q}$, we choose to reconstruct the primitive variables $\boldsymbol{W} = {}^t(\alpha_1\rho_1, \alpha_2\rho_2, \boldsymbol{u}, p, \alpha_1)$, thus we set

$$\begin{cases} \boldsymbol{W}_{ij} = \boldsymbol{W}_i + \frac{1}{2}(\nabla\boldsymbol{W})_{ij}\cdot\boldsymbol{ij} & \text{(a)} \\ \boldsymbol{W}_{ji} = \boldsymbol{W}_j - \frac{1}{2}(\nabla\boldsymbol{W})_{ji}\cdot\boldsymbol{ij} & \text{(b)} \end{cases} \tag{47}$$

The approximate nodal gradients $(\nabla\boldsymbol{W})_{ij}$ and $(\nabla\boldsymbol{W})_{ji}$ are obtained using a ζ combination of centered and fully upwind gradients:

$$(\nabla\boldsymbol{W})_{ij}\cdot\boldsymbol{ij} = (1-\zeta)(\nabla\boldsymbol{W})^{\mathrm{Cent}}_{ij}\cdot\boldsymbol{ij} + \zeta(\nabla\boldsymbol{W})^{\mathrm{Upw}}_{ij}\cdot\boldsymbol{ij} \tag{48}$$

The centered gradient $(\nabla\boldsymbol{W})^{\mathrm{Cent}}_{ij}$ is defined by

$$(\nabla\boldsymbol{W})^{\mathrm{Cent}}_{ij}\cdot\boldsymbol{ij} = \boldsymbol{W}_j - \boldsymbol{W}_i \tag{49}$$

The fully upwind gradient is computed according to the definition of the downstream and upstream triangles which can be associated with an edge $[S_i, S_j]$

$$(\nabla\boldsymbol{W})^{\mathrm{Upw}}_{ij} = \nabla\boldsymbol{W}^G T_{ij} \tag{50}$$

where $\nabla\boldsymbol{W}^G T = \sum_{k\in T}\boldsymbol{W}_k\nabla N^T_k$ is the P1 Galerkin gradient on triangle T and where T_{ij} and T_{ji} are, respectively, the upstream and downstream triangles (see Fig. 1). For every segment $[S_i, S_j]$, we can define two elements T_{ij} and T_{ji} to be such that $S_i + \lambda\boldsymbol{ij} \in T_{ij}$ and $S_j + \lambda\boldsymbol{ji} \in T_{ji}$ provided λ is small enough positive number. One can notice that for boundary edges, it can occur that the upwind or downwind triangles do not exist. Our choice has been to keep a first-order scheme in these particular cases.

Remark. In practice, the definition of these triangles is not trivial and a simplest approach involves computing the

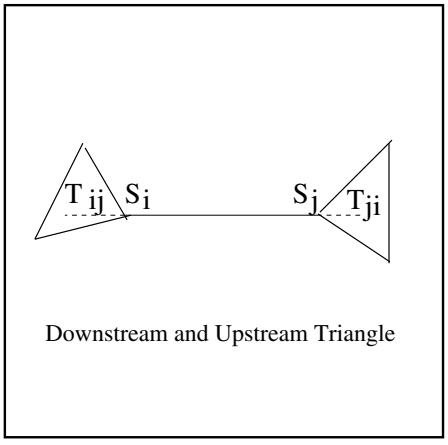

Fig. 1. Definition of upwind and downwind triangle associated to edge $[i, j]$.

gradients $(\nabla \boldsymbol{W})_{ij}$ at the node i with the following averaged formula:

$$(\nabla \boldsymbol{W})_{ij} = \frac{1}{A_i} \sum_{Ti \in T} \frac{A(T)}{3} \sum_{k \in T} \boldsymbol{W}_k \nabla N_k^T$$

which represents an average of the P1 Galerkin gradient on all triangles which contain the node i. This approach is less accurate but easier to implement because it does not require the computation of the upwinding triangles. Unfortunately, this method does not appear very robust for our problems and especially for interface ones with high density ratio between the two fluids. This is the reason why we have adopted the upwinding triangles method.

ζ is a parameter of upwinding included in interval [0, 1]. In the test cases presented in the sequel, we took either $\zeta = 1/2$ or $\zeta = 1/3$. The scheme described above is not monotone. It can create extrema particularly in the case of transonic and supersonic flows. To reduce the oscillations in the solution a slope limiting procedure can be used. Here we describe two classical procedures.

Van Albada–Van Leer limiter: This limitation allows to compute an upwind coefficient $\zeta^{\lim} \in [0, 1]$ which gives a good compromise between center and upwind gradients. The approximation writes

$$\begin{cases} \boldsymbol{W}_{ij} = \boldsymbol{W}_i + \frac{1}{2} \mathrm{Lim}_{\mathrm{vavl}} \left((\nabla \boldsymbol{W})_{ij}^{\mathrm{Upw}}, (\nabla \boldsymbol{W})_{ij}^{\mathrm{Cent}} \right) \cdot \boldsymbol{ij} & \text{(a)} \\ \boldsymbol{W}_{ji} = \boldsymbol{W}_j - \frac{1}{2} \mathrm{Lim}_{\mathrm{vavl}} \left((\nabla \boldsymbol{W})_{ji}^{\mathrm{Upw}}, (\nabla \boldsymbol{W})_{ji}^{\mathrm{Cent}} \right) \cdot \boldsymbol{ij} & \text{(b)} \end{cases} \tag{51}$$

where

$$\begin{aligned} &\mathrm{Lim}_{\mathrm{vavl}}(a, b) = \zeta^{\lim} a + (1 - \zeta^{\lim}) b \quad \text{if } ab > 0 \\ &\mathrm{Lim}_{\mathrm{vavl}}(a, b) = 0 \quad \text{if } ab < 0 \end{aligned} \tag{52}$$

with

$$\zeta^{\lim} = \frac{b^2 + \varepsilon}{a^2 + b^2 + 2\varepsilon}, \quad \varepsilon \ll 1 \tag{53}$$

Spekreijse limiter: This procedure uses the ratio between centered and upwind gradients. It is defined by

$$\begin{cases} \boldsymbol{W}_{ij} = \boldsymbol{W}_i + \frac{1}{2} \mathrm{Lim}_{\mathrm{spek}} \left((\nabla \boldsymbol{W})_{ij}^{\mathrm{Upw}}, (\nabla \boldsymbol{W})_{ij}^{\mathrm{Cent}} \right) \cdot \boldsymbol{ij} & \text{(a)} \\ \boldsymbol{W}_{ji} = \boldsymbol{W}_j - \frac{1}{2} \mathrm{Lim}_{\mathrm{spek}} \left((\nabla \boldsymbol{W})_{ji}^{\mathrm{Upw}}, (\nabla \boldsymbol{W})_{ji}^{\mathrm{Cent}} \right) \cdot \boldsymbol{ij} & \text{(b)} \end{cases} \tag{54}$$

where

$$\begin{aligned} &\mathrm{Lim}_{spek}(a, b) \\ &\quad = \max \left(0, \min \left(2 \frac{b + \varepsilon}{a + \varepsilon}, \min \left(\zeta + (1 - \zeta) \frac{b + \varepsilon}{a + \varepsilon}, 2 \right) \right) \right), \\ &\quad \varepsilon \ll 1 \end{aligned} \tag{55}$$

The Van Albada–Van Leer limiter is slightly more diffusive than the Spekreijse limiter but it is much more robust. In practice, we have used the Van Albada–Van Leer limiter with $\zeta^{\lim} = 1/2$ for the implicit computations reported in this paper and the Spekreijse limiter with $\zeta = 1/3$ for the reference explicit computation done in Section 4.1.

4. Numerical results

In this section, we present a set of two-dimensional tests which show that preconditioning reduces the diffusion of the original upwind scheme and allows to recover a better accuracy when computing low Mach number two-phase flows.

4.1. Bubble ascension

The first test shows the ascension of a light air-bubble under the effect of gravity in a closed box filled with water. We emphasize that a realistic simulation of this problem would have required the use of a capillarity model to take into account the effects of surface tension. However, here, our goal is not to obtain physically realistic results but instead to compare preconditioned dissipation with the classical upwind one. Initially the bubble is at rest and the pressure field has an hydrostatic profile. The box is 2 m large and 2 m high and the mesh is composed of 100×100 points. Although it seems simple, this computation presents several numerical difficulties. The first one is that the Mach number in this computation is extremely low (it is equal to zero at time $t = 0$ and increases slightly up to a value of 10^{-1} in the course of the computation). The second one is that the density ratio between the two fluids is equal to 1000. And the last numerical difficulty is that the equations of state of the two pure fluids are very different. They are

$$\begin{cases} p = (\gamma_1 - 1)\rho_1 \varepsilon_1 - \gamma_1 \pi_1 \quad \text{with } \gamma_1 = 1.4 \quad \text{and} \quad \pi_1 = 0 \quad \text{air} & \text{(a)} \\ p = (\gamma_2 - 1)\rho_2 \varepsilon_2 - \gamma_2 \pi_2 \quad \text{with } \gamma_2 = 4.4 \quad \text{and} \quad \pi_2 = 6 \times 10^8 \\ \quad \text{water} & \text{(b)} \end{cases} \tag{56}$$

This difficult test will show the effect of the preconditioning since the flow is very close to the incompressible regime. Fig. 2 shows the isovalues of the volume fraction at time = 0 s, 0.15 s, 0.35 s, 0.55 s, 0.75 s, 1.0 s for the classical upwind scheme while Fig. 3 shows the results at the same times with the preconditioned numerical method. The implicit time advancing method has been used with a CFL equal to 2.5. The space discretization has used the MUSCL technique described in Section 3.3, with $\zeta = 1/2$ and the Van Albada–Van Leer limiter. We can observe that very large differences develop during the course of the simulation. In particular, after time $t = 0.55$ s, the two results have almost no resemblance.

In order to demonstrate that preconditioning of the numerical dissipation improves the accuracy of the results, we have repeated this computation on a finer mesh of 400×400 points. Moreover, this fine mesh computation has been done with an explicit second-order space and time

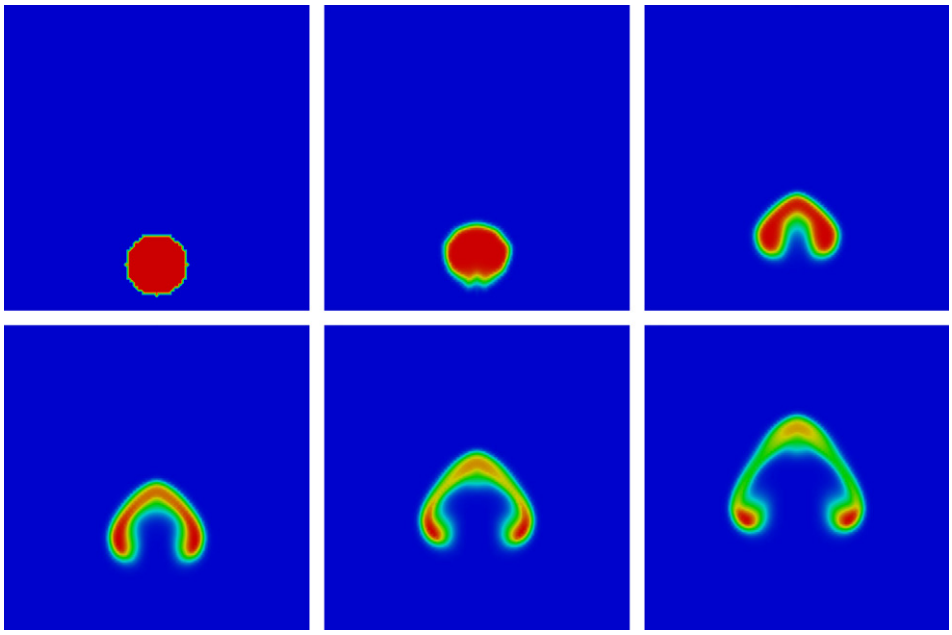

Fig. 2. Bubble ascension: isovalues of the volume fraction for the 100×100 mesh computation: classical upwind scheme.

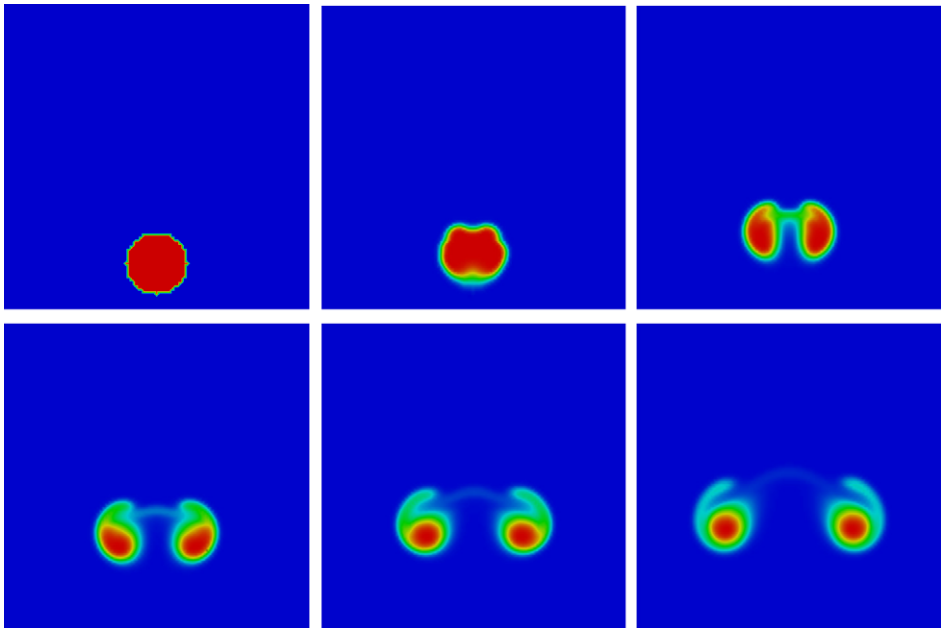

Fig. 3. Bubble ascension: isovalues of the volume fraction for the 100×100 mesh computation: preconditioned scheme with $\beta = 0.1$.

scheme. Namely, the time integration has used the three stage TVD Runge–Kutta discretization described in [11],

$$\begin{cases} \boldsymbol{Q}_i^{(1)} = \boldsymbol{Q}_i^n + \Delta t \mathbf{L}(\boldsymbol{Q}_i^n) & \text{(a)} \\ \boldsymbol{Q}_i^{(2)} = \frac{3}{4}\boldsymbol{Q}_i^n + \frac{1}{4}\boldsymbol{Q}_i^{(1)} + \frac{1}{4}\Delta t \mathbf{L}(\boldsymbol{Q}_i^{(1)}) & \text{(b)} \\ \boldsymbol{Q}_i^{n+1} = \frac{1}{3}\boldsymbol{Q}_i^n + \frac{2}{3}\boldsymbol{Q}_i^{(2)} + \frac{2}{3}\Delta t \mathbf{L}(\boldsymbol{Q}_i^{(2)}) & \text{(c)} \end{cases} \tag{57}$$

while the space discretization has used the MUSCL technique described in Section 3.3, with $\zeta = 1/3$ and the Spekreijse limiter. The results of this computation are shown in Fig. 4. Although the results of this fine mesh computation are not totally identical to those of Fig. 3, one can note the close similarity between these results and the one obtained with the preconditioned upwind scheme.

4.2. Broken dam problem

Here we present a computation of the well-known broken dam problem of Martin and Moyce [7]. Initially a water column with $a = 0.06$ m wide and $\eta^2 a = 0.12$ m high is a rest. Under the effect of the gravity $g = 9.81$ m s^{-2}, the column collapses. All the boundaries are solid walls. The

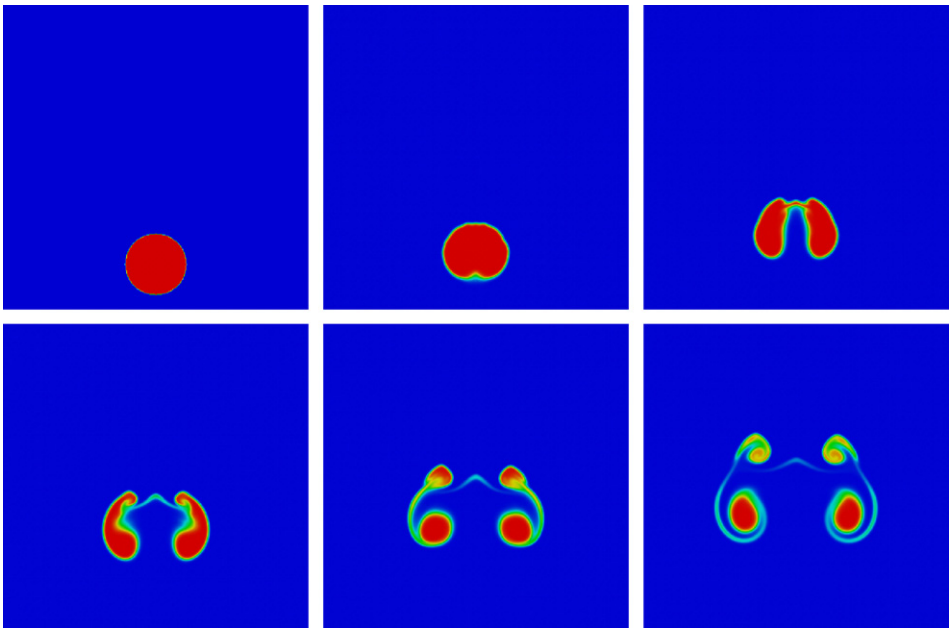

Fig. 4. Bubble ascension: isovalues of the volume fraction for the 400×400 fine mesh explicit computation.

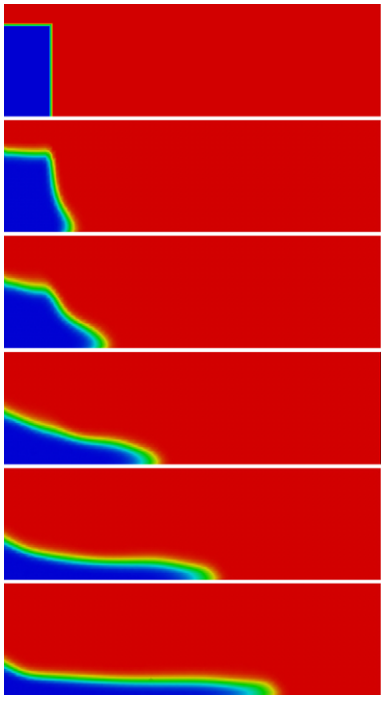

Fig. 5. Broken dam problem: isovalues of the volume fraction: classical upwind scheme.

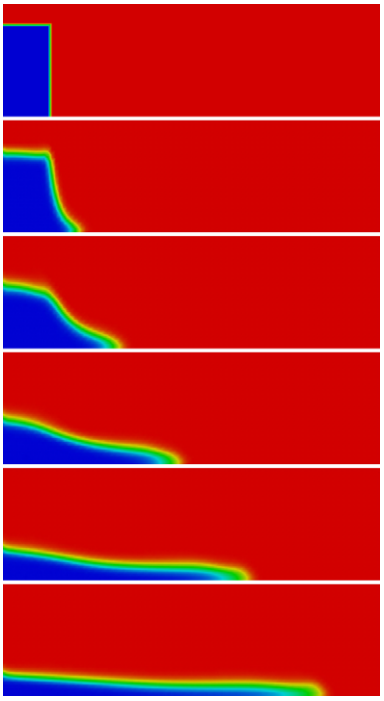

Fig. 6. Broken dam problem: isovalues of the volume fraction: preconditioned scheme with $\beta = 0.1$.

mesh we have used for this test, is regular with $\Delta_x = \Delta_z = 5 \times 10^{-3}$m. The Mach number during the computation is low and of the order of 1×10^{-1}. The implicit scheme has been used with a CFL number equal to 2.5 in order to compute with a sufficient accuracy the unsteady pattern of the flow. The linear system is solved by an iterative method with a linear residual $\theta = 1 \times 10^{-2}$. The space discretization has used the MUSCL technique with $\zeta = 1/2$ and the Van Albada–Van Leer limiter. We compute the solution with the standard and the preconditioned method. For the preconditioned method, the parameter of the Turkel's matrix β is chosen equal to 0.1 and remains constant in space and time.

Figs. 5 and 6 show the isovalues of the volume fraction at the different dimensionless times $t\sqrt{2g/a} = 0, 1.19, 1.98, 2.97, 4.02, 5.09$ corresponding to the physical

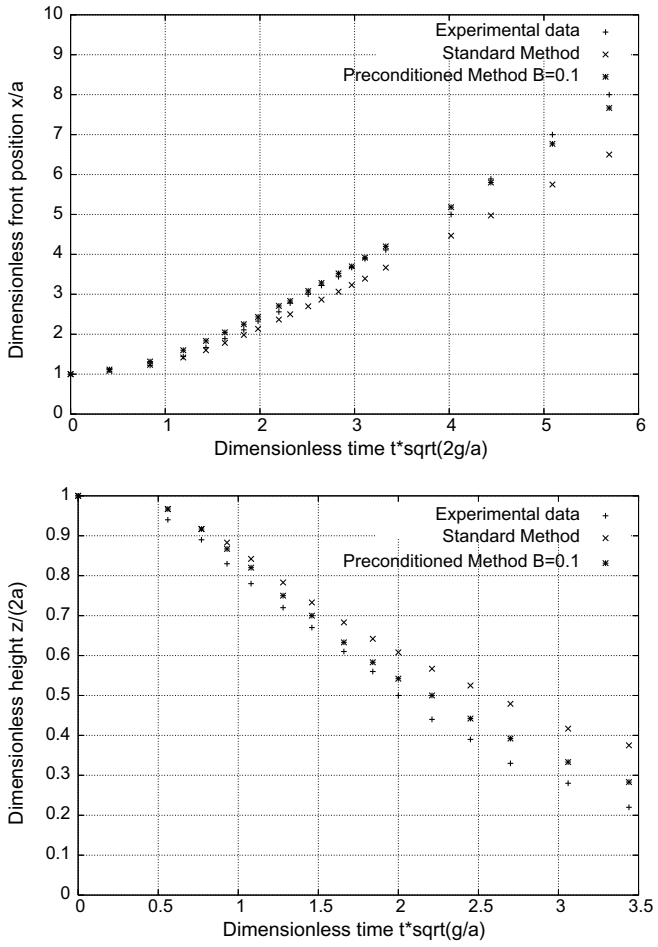

Fig. 7. Comparison between numerical solutions of the classical and preconditioned scheme and experimental results for the broken dam problem. Front position (top) and height of the column (bottom).

times $t = 0$, 0.066 s, 0.109 s, 0.164 s, 0.222 s, 0.281 s, for the standard (Fig. 5) and the preconditioned method (Fig. 6). It is clear that the upwind preconditioned scheme predicts a faster development of the flow and for instance the front position at time 0.281 s is clearly in advance with respect to the results obtained with the standard scheme.

To quantify the difference between the two schemes, we compare in Fig. 7, the two solutions with the experimental results of [7], for the front position $x/a = F_1\left(\eta^2, t\sqrt{2g/a}\right)$ and the height of the column $z/(\eta^2 a) = F_2\left(\eta^2, t\sqrt{g/a}\right)$. It is clear that the preconditioned method is more accurate than the standard one. For example at time $t\sqrt{2g/a} = 2.97$ the error compared to the experimental data for the front position is the order of 1% for the preconditioned method while it is the order of 10% for the classical upwind scheme.

4.3. Two-phase flow in a nozzle

Finally we present a sequence of computations of two-phase flows in a symmetric nozzle where the Mach number tends to zero. These computations are similar to the ones presented in [4] in single phase situation. The implicit scheme has been used with a CFL number equal to the inverse of the nonlinear residual of the mixture density $\mathrm{CFL} = 1/\mathrm{Res}(\rho)$ and at maximum equal to 10^6. The discrete solutions presented are the one obtained at convergence, i.e., for a residual equal to 10^{-9}. For the preconditioned method in this case, the parameter β is not taken as a constant but locally computed at each interface of the mesh and at each time step.

In these computations, an air–water two phase mixture defined by $(\alpha_1^\infty = 0.5, \rho_1^\infty = 1\ \mathrm{kg\ m^{-3}}, \rho_2^\infty = 1000\ \mathrm{kg\ m^{-3}})$ is injected in the nozzle with an horizontal imposed velocity equal to $u^\infty = 1\ \mathrm{m\ s^{-1}}$. The law states (56) for air and water are the same than previously and a representative Mach number of the flow is defined by

$$Ma_*^2 = \frac{(u^\infty)^2}{(\hat{a}^\infty)^2} = \frac{1}{(\hat{a}^\infty)^2} \tag{58}$$

Then the inlet pressure is taken as solution of equation $Ma_*^2 - 1/(\hat{a}^\infty)^2 = 0$ which can be rewritten using the equations of state of the two fluids:

$$Ma_*^2 - (\alpha_1^\infty \rho_1^\infty + (1-\alpha_1^\infty)\rho_2^\infty) \times \left(\frac{\alpha_1^\infty}{\gamma_1(p^\infty + \pi_1)} + \frac{1-\alpha_1^\infty}{\gamma_2(p^\infty + \pi_2)}\right) = 0 \tag{59}$$

We are interested in the situation where Ma_* tends to zero. In this case, the asymptotic analysis given in Section 2 applies and shows that the equations governing the flow are the two-phase incompressible Euler equations (14). Thus if we take at time $t = 0, \alpha_1(x,0) = 0.5$ for all x, we will get $\alpha_1(x,t) = 0.5$ for all x and $t > 0$ and (1) is simply the incompressible Euler equation with a constant density given by $(\rho_1 + \rho_2)/2$. We then expect that the limit solution of (1) will be given by an incompressible potential flow of density $(\rho_1 + \rho_2)/2$. In particular, the solution has to be symmetric with respect to the axis of the nozzle. To test the preconditioned scheme with respect to the classic non-preconditioned one, we realize three computations, respectively, at $Ma_* = 0.1, Ma_* = 0.01$ and $Ma_* = 0.001$.

Fig. 8 shows the isovalues of the normalized pressure $p - p_{\min}/p_{\max} - p_{\min}$ for the discrete stationary solutions obtained. Fig. 9 shows the profile of pressure in the upper and lower boundaries of the nozzle. We present from left to right the results obtained with the classical and the preconditioned scheme.

Fig. 9 shows clearly that the solution given by the classical discretization is not symmetric and consequently could not be a reasonable approximation of the incompressible solution. In addition, one can notice that the pressure fluctuations with the classic scheme (of order Ma_*) are larger than which obtained with the preconditioned one (of order Ma_*^2). To illustrate this difference in the behaviour of the pressure fluctuations, we plot in the first and second column of Fig. 9 the result for the classic and preconditioned method with the same pressure unit. We could note

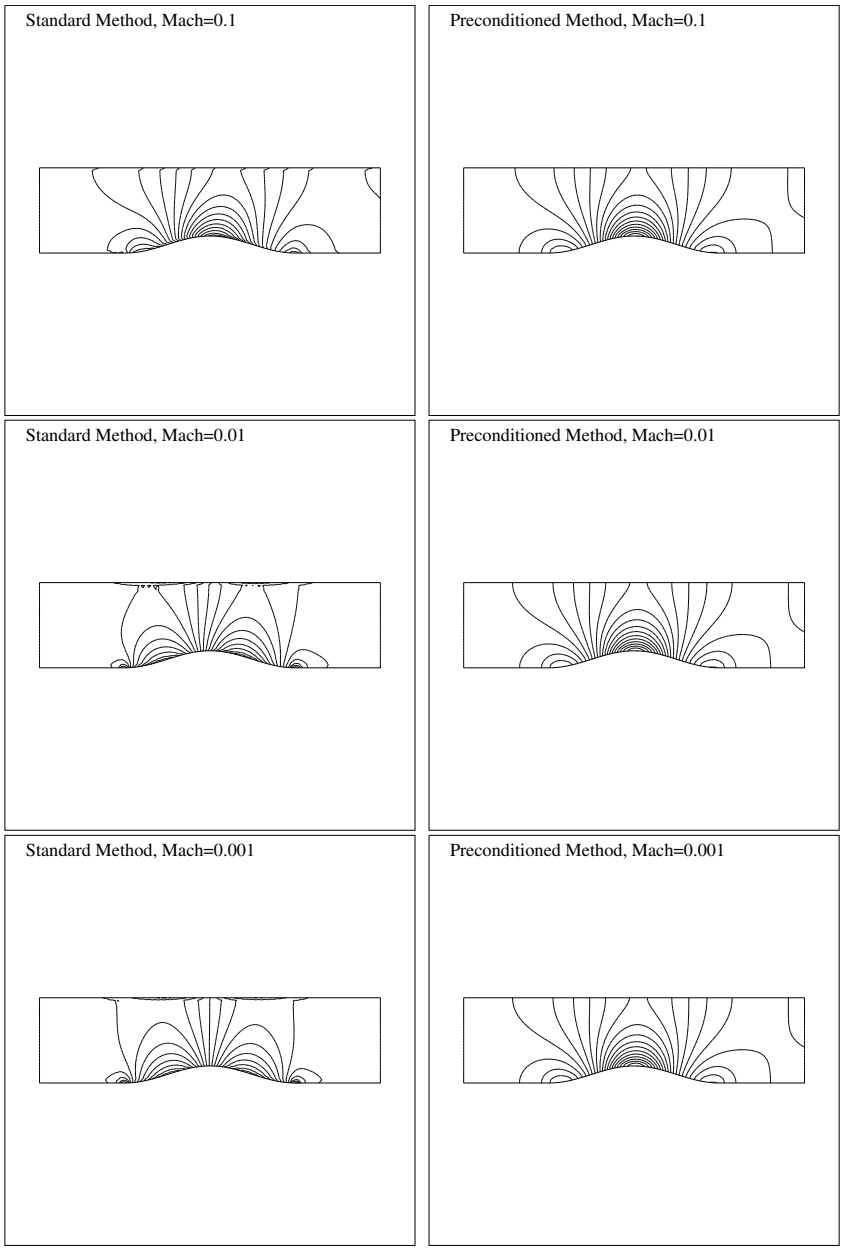

Fig. 8. Isovalues of the normalized pressure, on a 3277 node mesh at $Ma_\infty = 0.1$ (top), $Ma_\infty = 0.01$ (middle), $Ma_\infty = 0.001$ (bottom). Classic (left) and preconditioned scheme (right).

for instance that for $Ma_* = 10^{-3}$ it is difficult to observe the fluctuations (of order Ma_*^2) given by the preconditioned method. In order to illustrate the behaviour of the preconditioned scheme in the zero Mach number limit, the last column of Fig. 9 presents the pressure profile with y-scale adapted to the amplitude of the pressure fluctuations. It can be seen that the results are almost identical.

As the Mach number decreases, results of the classic scheme become worse (see Fig. 8) and do not converge to a reasonable approximation of the incompressible solution. In contrast the solutions of the preconditioned method converge to an unique symmetric solution and the pressure fluctuations scale with the square of the Mach number Ma_*^2 in agreement with the asymptotic behaviour of the continuous equations. This shows the necessity of using preconditioning method when computing low Mach two-phase flows.

5. Conclusion

Since the convective part of hyperbolic models of two-phase flow derives from the one-phase Euler equations, one can suspect that a loss of accuracy will affect the results when trying to solve these models in the low Mach number regime by standard finite volume upwind procedures. We have analyzed this situation for a five equation two-phase flow model proposed in [6,8]. First, an asymptotic analysis of this model has been performed and has allowed to exhi-

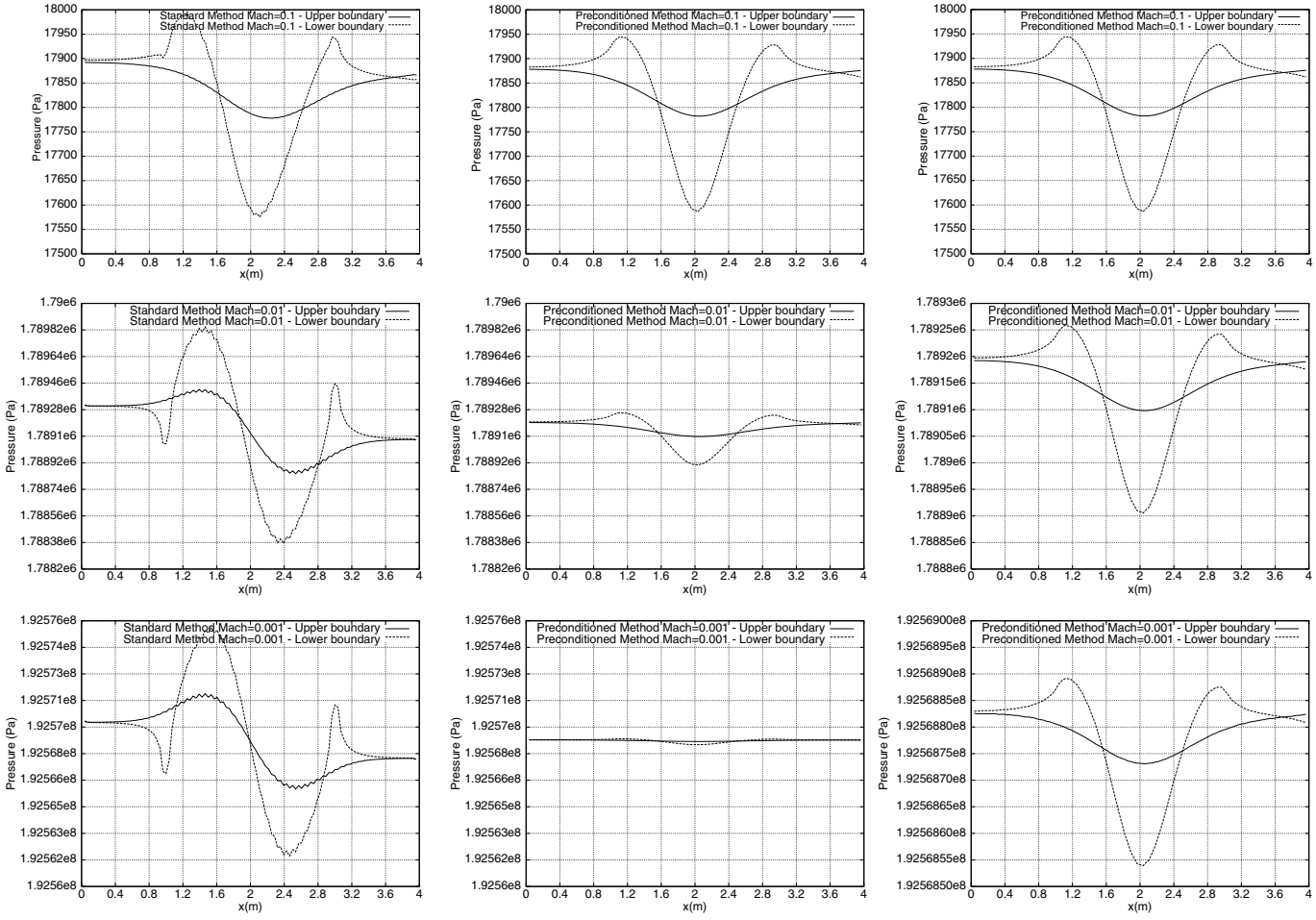

Fig. 9. Profile pressure in the upper and lower boundaries, on a 3277 node mesh at $Ma_\infty = 0.1$ (top), $Ma_\infty = 0.01$ (middle), $Ma_\infty = 0.001$ (bottom). Classic (left) and preconditioned scheme (middle). The right column presents a zoom of the middle column results.

bit the equations that the solutions satisfy in the low Mach number limit. In particular, we have shown that these limit equations are very close to the incompressible single phase equations and that the pressure scales with the square of the Mach number. From a numerical point of view, we have proposed an implicit extension of the Godunov type schemes that we have applied to this model. Then using the close similarity between the mathematical structure of this two-phase model and the structure of the single phase Euler equations, we have used the strategy presented in [4] to correct the numerical dissipation by solving a *preconditioned* Riemann problem. The numerical results have shown that this method clearly improves the accuracy of upwind finite volume methods in the low Mach regime. For instance, in the case of the broken dam problem, the error has been reduced by a factor 10 with respect to the solution obtained by a classical upwind scheme at virtually no cost.

The extension of this method to other more general two-phase flow models would be of great practical and theoretical interest since in general for two-phase flows, at least one of the fluid (the liquid) is close to the incompressible limit. However, for hyperbolic models including two velocities and two pressures, since, several Mach numbers can be defined, the situation is far from being understood even from the point of view of formal asymptotic analysis and a lot of work remains to be done.

Appendix A. Jacobian matrix

The subject of this section is to compute the Jacobian matrix of model (1) and we first need to compute the differential of the pressure in term of conservative variables. So let us write $\rho_k\varepsilon_k = \rho_k\varepsilon_k(\rho_k, p)$ and introduce the coefficients $\delta_k = (\partial\rho_k\varepsilon_k/\partial\rho_k)_p$ and $\xi_k = (\partial\rho_k\varepsilon_k/\partial p)_{\rho_k}$. The differential $\mathrm{d}(\rho_k\varepsilon_k)$ writes

$$\mathrm{d}(\rho_k\varepsilon_k) = \delta_k \mathrm{d}\rho_k + \xi_k \mathrm{d}p \quad \text{for } k = 1, 2 \tag{A.1}$$

Then we use the Gibb's relation for each phase:

$$\mathrm{d}\varepsilon_k = T_k \mathrm{d}s_k + \frac{p_k}{\rho_k^2}\mathrm{d}\rho_k \quad \text{for } k = 1, 2 \tag{A.2}$$

where T_k is the temperature of phase k. Introducing $h_k = \varepsilon_k + p/\rho_k$ which stand for the specific phase enthalpies, the Gibb's relation (A.2) can be rewritten under the form:

$$\mathrm{d}(\rho_k\varepsilon_k) = \rho_k T_k \mathrm{d}s_k + h_k \mathrm{d}\rho_k \quad \text{for } k = 1,2 \tag{A.3}$$

Now writing equality of (A.3)–(A.1), we get the well-known relations:

$$a_k^2 = \left(\frac{\partial p}{\partial \rho_k}\right)_{s_k} = \frac{h_k - \delta_k}{\xi_k} \quad \text{and} \quad \left(\frac{\partial p}{\partial s_k}\right)_{\rho_k} = \frac{\rho_k T_k}{\xi_k} \quad \text{for } k = 1,2 \tag{A.4}$$

where a_k are the phase sound speeds.

Now let us compute the differential of the pressure. Using the definition of the internal mixture energy $\rho\varepsilon = \sum_{k=1}^{2}\alpha_k\rho_k\varepsilon_k$ and summing the differentials (A.1) for the two phases, we get after some manipulations:

$$\sum_{k=1}^{2}\alpha_k\xi_k \mathrm{d}p = -\sum_{k=1}^{2}\delta_k \mathrm{d}(\alpha_k\rho_k) + \mathrm{d}(\rho\varepsilon) - \sum_{k=1}^{2}(\rho_k\varepsilon_k - \rho_k\delta_k)\mathrm{d}\alpha_k \tag{A.5}$$

Now introducing the new parameter $\xi = \sum_{k=1}^{2}\alpha_k\xi_k$ and also the relation $\mathrm{d}(\rho\varepsilon) = \boldsymbol{u}^2/2\sum_{k=1}^{2}d(\alpha_k\rho_k) - \boldsymbol{u}\cdot\mathrm{d}(\rho\boldsymbol{u}) + \mathrm{d}(\rho e)$, we get the differential of the pressure in term of conservative variables:

$$\begin{cases} \mathrm{d}p = \sum_{k=1}^{2}\frac{1}{\xi}(\frac{u^2}{2} - \delta_k)\mathrm{d}(\alpha_k\rho_k) - \frac{u}{\xi}\cdot\mathrm{d}(\rho\boldsymbol{u}) + \frac{1}{\xi}\mathrm{d}(\rho e) \\ \qquad + \frac{1}{\xi}(\rho_2(\varepsilon_2 - \delta_2) - \rho_1(\varepsilon_1 - \delta_1))\mathrm{d}\alpha_1 \end{cases} \tag{A.6}$$

And the purpose is to compute, for all normalized vector $\boldsymbol{\eta} = {}^t(\eta_x, \eta_y)$, the eigenelements of the matrix:

$$D_c(\boldsymbol{Q}) = \frac{\partial \boldsymbol{F}(\boldsymbol{Q})\cdot\boldsymbol{\eta}}{\partial \boldsymbol{Q}} + \boldsymbol{B}(\boldsymbol{Q})\frac{\partial \boldsymbol{u}\cdot\boldsymbol{\eta}}{\partial \boldsymbol{Q}} \tag{A.7}$$

So let us consider the rotation matrix θ which allows to pass from $\boldsymbol{Q}$ in the global basis to $\tilde{\boldsymbol{Q}} = \theta\boldsymbol{Q} = {}^t(\alpha_1\rho_1, \alpha_2\rho_2, \rho v_n, \rho v_t, \rho e, \alpha_1)$ in the local basis $(\boldsymbol{\eta}, \boldsymbol{\eta}^\perp)$.

v_n, v_t are, respectively, normal and tangential components of the vector velocity and given by

$$\begin{cases} v_n = \boldsymbol{u}\cdot\boldsymbol{\eta} & \text{(a)} \\ v_t = \boldsymbol{u}\cdot\boldsymbol{\eta}^\perp & \text{(b)} \end{cases} \tag{A.8}$$

After computations, the matrix $D_c(\boldsymbol{Q})$ can be written under the form:

$$\begin{pmatrix} Y_2 v_n & -Y_1 v_n & Y_1\eta_x & Y_1\eta_y \\ -Y_2 v_n & Y_1 v_n & Y_2\eta_x & Y_2\eta_y \\ B_1\eta_x - u v_n & B_2\eta_x - u v_n & (1-\frac{1}{\xi})u\eta_x + v_n & (1-\frac{1}{\xi})v\eta_x - v_t \\ B_1\eta_y - v v_n & B_2\eta_y - v v_n & (1-\frac{1}{\xi})u\eta_y + v_t & (1-\frac{1}{\xi})v\eta_y + v_n \\ (B_1 - H)v_n & (B_2 - H)v_n & H\eta_x - \frac{u v_n}{\xi} & H\eta_y - \frac{v v_n}{\xi} \\ -A v_n/\rho & -A v_n/\rho & A\eta_x/\rho & A\eta_y/\rho \end{pmatrix} \begin{matrix} 0 & 0 \\ 0 & 0 \\ \frac{\eta_x}{\xi} & M\eta_x \\ \frac{\eta_y}{\xi} & M\eta_y \\ (1+\frac{1}{\xi})v_n & M v_n \\ 0 & v_n \end{matrix} \tag{A.9}$$

where $Y_k = \alpha_k\rho_k/\rho$ stand for the mass fractions and $H = \sum_{k=1}^{2}Y_k H_k = e + p/\rho$ with $H_k = h_k + \boldsymbol{u}^2/2$ the specific total phase enthalpies. Then the other coefficients B_k, M, A are defined by

$$\begin{cases} B_k = \frac{1}{\xi}(\frac{u^2}{2} - \delta_k) & \text{for } k = 1,2 \quad \text{(a)} \\ M = \frac{1}{\xi}(\rho_2(\varepsilon_2 - \delta_2) - \rho_1(\varepsilon_1 - \delta_1)) & \text{(b)} \\ A = \alpha_1\alpha_2\frac{\rho_1 a_1^2 - \rho_2 a_2^2}{\sum_{k=1}^{2}\alpha_{k'}\rho_k a_k^2} & \text{(c)} \end{cases} \tag{A.10}$$

The matrix $D_c(\boldsymbol{Q})$ is diagonalizable with three real distinct eigenvalues:

$$\begin{cases} \lambda_1(\boldsymbol{Q}) = v_n - \hat{a} \\ \lambda_2(\boldsymbol{Q}) = \lambda_3(\boldsymbol{Q}) = \lambda_4(\boldsymbol{Q}) = \lambda_5(\boldsymbol{Q}) = v_n \\ \lambda_6(\boldsymbol{Q}) = v_n + \hat{a} \end{cases} \tag{A.11}$$

where the value of the sound speed $\hat{a}$ is defined by the expression:

$$\rho\hat{a}^2 = \frac{1}{\xi}\sum_{k=1}^{2}\alpha_k\xi_k\rho_k a_k^2 + MA \tag{A.12}$$

which is equivalent to the averaged formula (4) given in Section 2. In effect using expressions (A.10.b) and (A.10.c) and also introducing $\rho_2\varepsilon_2 - \rho_1\varepsilon_1 = \rho_2 h_2 - \rho_1 h_1$ which is only valid because the two phases have the same pressure, we get

$$\rho\hat{a}^2 = \frac{1}{\xi}\sum_{k=1}^{2}\alpha_k\xi_k\rho_k a_k^2 + \frac{1}{\xi}(\rho_2(h_2 - \delta_2) - \rho_1(h_1 - \delta_1))\alpha_1\alpha_2\frac{\rho_1 a_1^2 - \rho_2 a_2^2}{\sum_{k=1}^{2}\alpha_{k'}\rho_k a_k^2} \tag{A.13}$$

Using the relation (A.4) for the phase sound speed $\xi_k a_k^2 = h_k - \delta_k$, we get

$$\rho\hat{a}^2 = \frac{1}{\xi}\sum_{k=1}^{2}\alpha_k\xi_k\rho_k a_k^2 + \frac{1}{\xi}(\xi_2\rho_2 a_2^2 - \xi_1\rho_1 a_1^2)\alpha_1\alpha_2\frac{\rho_1 a_1^2 - \rho_2 a_2^2}{\sum_{k=1}^{2}\alpha_{k'}\rho_k a_k^2} \tag{A.14}$$

And after manipulations, we check the following expression which is clearly equivalent to the averaged formula (4) given in Section 2:

$$\rho\hat{a}^2 = \frac{\rho_1 a_1^2 \rho_2 a_2^2}{\sum_{k=1}^{2}\alpha_{k'}\rho_k a_k^2} \tag{A.15}$$

Then, the right eigenvectors $r_i(\boldsymbol{Q})$ (for $i \in \{1,\ldots,6\}$) of the matrix which verify the relation $D_c(\boldsymbol{Q})r_i(\boldsymbol{Q}) = \lambda_i(\boldsymbol{Q})r_i(\boldsymbol{Q})$ can be chosen as

$$r_1=\begin{pmatrix} Y_1\\ Y_2\\ u-\hat{a}\eta_x\\ v-\hat{a}\eta_y\\ H-\hat{a}v_{\mathrm{n}}\\ A/\rho \end{pmatrix}\quad r_2=\begin{pmatrix} 1\\ 0\\ u\\ v\\ \boldsymbol{u}^2/2+\delta_1\\ 0 \end{pmatrix}\quad r_3=\begin{pmatrix} 0\\ 1\\ u\\ v\\ \boldsymbol{u}^2/2+\delta_2\\ 0 \end{pmatrix}$$

$$r_4=\begin{pmatrix} 0\\ 0\\ -\eta_y\\ \eta_x\\ v_{\mathrm{t}}\\ 0 \end{pmatrix}\quad r_5=\begin{pmatrix} 0\\ 0\\ 0\\ 0\\ -M\xi\\ 1 \end{pmatrix}\quad r_6=\begin{pmatrix} Y_1\\ Y_2\\ u+a\eta_x\\ v+\hat{a}\eta_y\\ H+\hat{a}v_{\mathrm{n}}\\ A/\rho \end{pmatrix} \tag{A.16}$$

We denote also by $l_i(\boldsymbol{Q})$ (for $i\in\{1,\dots,6\}$) the left eigenvectors which obey the relation ${}^tD_c(\boldsymbol{Q})l_i(\boldsymbol{Q})=\lambda_i(\boldsymbol{Q})l_i(\boldsymbol{Q})$. After normalization of the left and right eigenvectors to have ${}^tl_i(\boldsymbol{Q})\cdot r_j(\boldsymbol{Q})=\delta_{ij}$, we get

$$l_1=\frac{1}{2\hat{a}^2}\begin{pmatrix} B_1+\hat{a}v_{\mathrm{n}}\\ B_2+\hat{a}v_{\mathrm{n}}\\ -u/\xi-\hat{a}\eta_x\\ -v/\xi-\hat{a}\eta_y\\ 1/\xi\\ M \end{pmatrix}\quad l_2=\frac{1}{\hat{a}^2}\begin{pmatrix} \hat{a}^2-Y_1B_1\\ -Y_1B_2\\ Y_1u/\xi\\ Y_1v/\xi\\ -Y_1/\xi\\ -Y_1M \end{pmatrix}$$

$$l_3=\frac{1}{\hat{a}^2}\begin{pmatrix} -Y_2B_1\\ \hat{a}^2-Y_2B_2\\ Y_2u/\xi\\ Y_2v/\xi\\ -Y_2/\xi\\ -Y_2M \end{pmatrix}\quad l_4=\begin{pmatrix} -v_{\mathrm{t}}\\ -v_{\mathrm{t}}\\ -\eta_y\\ \eta_x\\ 0\\ 0 \end{pmatrix}$$

$$l_5=\frac{1}{\rho\hat{a}^2}\begin{pmatrix} -AB_1\\ -AB_2\\ Au/\xi\\ Av/\xi\\ -A/\xi\\ \rho\hat{a}^2-AM \end{pmatrix}\quad l_6=\frac{1}{2\hat{a}^2}\begin{pmatrix} B_1-\hat{a}v_{\mathrm{n}}\\ B_2-\hat{a}v_{\mathrm{n}}\\ -u/\xi+\hat{a}\eta_x\\ -v/\xi+\hat{a}\eta_y\\ 1/\xi\\ M \end{pmatrix} \tag{A.17}$$

Appendix B. Expression of the matrices R and R^{-1}

Here, we propose to compute the matrices R and R^{-1} which allow to switch from the "conservative" $\boldsymbol{Q}$ to the "entropic" variables $\boldsymbol{q}$. So let us start with the computation of the matrix R such as $\mathrm{d}\boldsymbol{q}=R\mathrm{d}\boldsymbol{Q}$. If we refer to Appendix A, we have

$$\mathrm{d}p=\sum_{k=1}^{2}B_k\mathrm{d}(\alpha_k\rho_k)-\frac{\boldsymbol{u}}{\xi}\cdot\mathrm{d}(\rho\boldsymbol{u})+\frac{1}{\xi}\mathrm{d}(\rho e)+M\mathrm{d}\alpha_1 \tag{B.1}$$

Now it is easily checked that the differential of the velocity $\boldsymbol{u}$ is given by

$$\mathrm{d}\boldsymbol{u}=-\frac{\boldsymbol{u}}{\rho}\sum_{k=1}^{2}\mathrm{d}(\alpha_k\rho_k)+\frac{1}{\rho}\mathrm{d}(\rho\boldsymbol{u}) \tag{B.2}$$

Then in order to compute the differential of the phase entropies s_k, we use the relation $\rho_kT_kds_k=\xi_k\mathrm{d}p-\xi_ka_k^2\mathrm{d}\rho_k$ which is a consequence of (A.1)–(A.4). Introducing the differential $\mathrm{d}p$ in this last relation, we get

$$\begin{cases} \mathrm{d}s_k=\frac{\xi_k}{\rho_kT_k}\sum_{k=1}^{2}B_k\mathrm{d}(\alpha_k\rho_k)-\frac{\xi_ka_k^2}{\alpha_k\rho_kT_k}\mathrm{d}(\alpha_k\rho_k)-\frac{\xi_k\boldsymbol{u}}{\xi\rho_kT_k}\cdot\mathrm{d}(\rho\boldsymbol{u})\\ +\frac{\xi_k}{\xi\rho_kT_k}\mathrm{d}(\rho e)+\frac{\xi_kM}{\rho_kT_k}\mathrm{d}\alpha_1+\frac{\xi_ka_k^2}{\alpha_kT_k}\mathrm{d}\alpha_k\quad\text{for } k=1,2 \end{cases} \tag{B.3}$$

Finally, using the definition of mass fractions $\rho Y_k=\alpha_k\rho_k$, we get

$$\rho\mathrm{d}Y_1=Y_2\mathrm{d}(\alpha_1\rho_1)-Y_1\mathrm{d}(\alpha_2\rho_2) \tag{B.4}$$

which complete the computation of the matrix R given by

$$\begin{pmatrix} B_1 & B_2 & -u/\xi & -v/\xi & 1/\xi & M\\ -u/\rho & -u/\rho & 1/\rho & 0 & 0 & 0\\ -v/\rho & -v/\rho & 0 & 1/\rho & 0 & 0\\ \frac{\xi_1(\alpha_1B_1-a_1^2)}{\alpha_1\rho_1T_1} & \frac{\xi_1B_2}{\rho_1T_1} & -\frac{\xi_1u}{\xi\rho_1T_1} & -\frac{\xi_1v}{\xi\rho_1T_1} & \frac{\xi_1}{\xi\rho_1T_1} & \frac{\xi_1\xi_2a_1^2\rho_2a_2^2}{\xi\alpha_1T_1\rho\hat{a}^2}\\ \frac{\xi_2B_1}{\rho_2T_2} & \frac{\xi_2(\alpha_2B_2-a_2^2)}{\alpha_2\rho_2T_2} & -\frac{\xi_2u}{\xi\rho_2T_2} & -\frac{\xi_2v}{\xi\rho_2T_2} & \frac{\xi_2}{\xi\rho_2T_2} & \frac{-\xi_1\xi_2\rho_1a_1^2a_2^2}{\xi\alpha_2T_2\rho\hat{a}^2}\\ Y_2/\rho & -Y_1/\rho & 0 & 0 & 0 & 0 \end{pmatrix} \tag{B.5}$$

Now the matrix R^{-1} such as $\mathrm{d}\boldsymbol{Q}=R^{-1}\mathrm{d}\boldsymbol{q}$ can be obtained with the same kind of manipulations and we do not give more details. The matrix R^{-1} is given by

$$\begin{pmatrix} \frac{Y_1}{\hat{a}^2} & 0 & 0 & -\frac{\alpha_1^2\rho_1T_1}{\xi_1a_1^2} & -\frac{\alpha_1\alpha_2\rho_1T_2}{\xi_2a_2^2} & \frac{\rho^2}{\rho_2}\\ \frac{Y_2}{\hat{a}^2} & 0 & 0 & -\frac{\alpha_1\alpha_2\rho_2T_1}{\xi_1a_1^2} & -\frac{\alpha_2^2\rho_2T_2}{\xi_2a_2^2} & -\frac{\rho^2}{\rho_1}\\ \frac{u}{\hat{a}^2} & \rho & 0 & -\frac{\alpha_1\rho T_1u}{\xi_1a_1^2} & -\frac{\alpha_2\rho T_2u}{\xi_2a_2^2} & \rho^2\left(\frac{u}{\rho_2}-\frac{u}{\rho_1}\right)\\ \frac{v}{\hat{a}^2} & 0 & \rho & -\frac{\alpha_1\rho T_1v}{\xi_1a_1^2} & -\frac{\alpha_2\rho T_2v}{\xi_2a_2^2} & \rho^2\left(\frac{v}{\rho_2}-\frac{v}{\rho_1}\right)\\ \frac{H}{\hat{a}^2} & \rho u & \rho v & \alpha_1T_1\left(\rho_1-\frac{\rho H}{\xi_1a_1^2}\right) & \alpha_2T_2\left(\rho_2-\frac{\rho H}{\xi_2a_2^2}\right) & \rho^2\left(\frac{H_1}{\rho_2}-\frac{H_2}{\rho_1}\right)\\ \frac{A}{\rho\hat{a}^2} & 0 & 0 & \frac{\alpha_1\alpha_2T_1}{\xi_1a_1^2} & -\frac{\alpha_1\alpha_2T_2}{\xi_2a_2^2} & \frac{\rho^2}{\rho_1\rho_2} \end{pmatrix} \tag{B.6}$$

Remark. The matrices $R=\partial\boldsymbol{q}/\partial\boldsymbol{Q}$ and $R^{-1}=\partial\boldsymbol{Q}/\partial\boldsymbol{q}$ are singular for $\alpha_k=0$ and $\alpha_k=1$. In practice for the numerical simulations, a pure fluid k is represented by $\alpha_k=1-\varepsilon$ with ε a small parameter. The result is not sensible to the choice of ε as we have checked numerically.

References

[1] Baer MR, Nunziato JW. A two-phase mixture theory for the deflagration-to-detonation transition (DDT) in reactive granular materials. J Multiphas Flows 1986;12:861–89.

[2] Clerc S. Numerical simulation of the homogeneous equilibrium model for two-phase flows. J Comput Phys 2000;161:354–75.

[3] Cournède PH, Debiez C, Dervieux A. A positive MUSCL scheme for triangulations. Technical report 3465, INRIA; 1998.

[4] Guillard H, Murrone A. On the behavior of upwind schemes in the low Mach number limit: II. Godunov type schemes. Comput Fluids 2004;33:655–75.

[5] Guillard H, Viozat C. On the behavior of upwind schemes in the low Mach number limit. Comput fluids 1999;28:63–96.

[6] Kapila AK, Menikoff R, Bdzil JB, Son SF, Stewart DS. Two-phase modelling of DDT in granular materials: reduced equations. Phys Fluids 2001;13:3002–24.

[7] Martin JC, Moyce WJ. An experimental study of the collapse of liquid columns on a rigid horizontal plane. Philos Trans Roy Soc London Ser A 1952;244:312–24.

[8] Murrone A, Guillard H. A five equation reduced model for compressible two phase flow problems. J Comput Phys 2005;202:664–98.

[9] Ransom VH, Hicks DL. Hyperbolic two-pressure models for two phase flow. J Comput Phys 1984;53:124–51.

[10] Saurel R, Abgrall R. A multiphase Godunov method for compressible multifluid and multiphase flows. J Comput Phys 1999;150:425–67.

[11] Shu CW, Osher S. Efficient implementation of essential non oscillatory shock capturing schemes. J Comput Phys 1988;77:439–71.

[12] Stewart HB, Wendroff B. Two-phase flow: models and methods. J Comput Phys 1984;56:363–409.

[13] Toro EF. Riemann solvers and numerical methods for fluid dynamics. Berlin: Springer-Verlag; 1997.

[14] Turkel E. Preconditioned methods for solving the incompressible and low speed compressible equations. J Comput Phys 1987;72:277–98.

[15] van Leer B. Towards the ultimate conservative difference scheme V. A second-order sequel to Godunov's method. J Comput Phys 1979;32:101–36.

[16] Viozat C. Calcul d'écoulements diphasiques dans une tuyère: Influence de la renormalisation du schéma de flux. Technical report SYSCO/LGLS/RT/00-014, CEA; 2000.

[17] Xu Shaojie, Stewart DS. Deflagration-to-detonation transition in porous energetic materials: a comparative model study. J Eng Math 1997;31:143–72.